

Multi-peaked localized states of DNLS in one and two dimensions

G. Kalosakas *

*Max Planck Institute for the Physics of Complex Systems,
Nöthnitzer Str. 38, Dresden, 01187, Germany*

Abstract

Multi-peaked localized stationary solutions of the discrete nonlinear Schrödinger (DNLS) equation are presented in one (1D) and two (2D) dimensions. These are excited states of the discrete spectrum and correspond to multi-breather solutions. A simple, very fast, and efficient numerical method, suggested by Aubry, has been used for their calculation. The method involves no diagonalization, but just iterations of a map, starting from trivial solutions of the anti-continuous limit. Approximate analytical expressions are presented and compared with the numerical results. The linear stability of the calculated stationary states is discussed and the structure of the linear stability spectrum is analytically obtained for relatively large values of nonlinearity.

Key words: DNLS, stationary states, multi-breathers, discrete spectrum

PACS: 05.45.-a, 02.70.-c, 03.75.Lm, 42.65.Tg

1 Introduction

The DNLS equation, Eq. (1), has been extensively used as a generic model for studying nonlinear effects (breathers, for example) in a discrete system [1,2,3,4,5,6,7,8,9,10,11,12]. In addition, specific applications have been proposed for the description of: *i)* local intramolecular stretching vibrations in symmetric polyatomic molecules [13], *ii)* arrays of coupled nonlinear optical waveguides [14], *iii)* interacting electron-lattice models [15,16] (or, equivalently, intramolecular excitation-phonon coupled systems [17,18,19]) in solid

* Fax: +49-351-871-1999. E-mail: georgek@pks.mpg.de

state physics, where localized solutions of DNLS correspond to polarons (vibrational polarons, respectively), and recently *iv*) Bose-Einstein condensates [20,21].

In DNLS the evolution of a complex probability amplitude Ψ_n at the site n of a d -dimensional lattice is given by

$$i \frac{d\Psi_n}{dt} = -V \sum_{\delta} \Psi_{n+\delta} + \chi |\Psi_n|^2 \Psi_n, \quad (1)$$

where V represents nearest neighbor coupling, χ is the strength of nonlinearity, and the sum over δ contains the nearest neighbors of the lattice site n . For example, in 1D is $\sum_{\delta} \Psi_{n+\delta} = \Psi_{n+1} + \Psi_{n-1}$, while in a 2D square lattice, if each lattice site n is represented by a pair (n_x, n_y) , is $\sum_{\delta} \Psi_{n+\delta} = \Psi_{n_x+1, n_y} + \Psi_{n_x-1, n_y} + \Psi_{n_x, n_y+1} + \Psi_{n_x, n_y-1}$.

The DNLS equation is derived from the Hamiltonian (assuming an infinite lattice, or periodic boundary conditions)

$$H = -V \sum_n \sum_{\delta} \Psi_n^* \Psi_{n+\delta} + \frac{\chi}{2} \sum_n |\Psi_n|^4. \quad (2)$$

There exist two conserved quantities during the DNLS dynamics: the Hamiltonian (2) and the norm

$$N = \sum_n |\Psi_n|^2. \quad (3)$$

A trivial transformation ($\Psi_n \rightarrow \Psi_n / \sqrt{N}$) connects the solutions of DNLS for an arbitrary norm N with those normalized to unity, through a rescaling of the nonlinearity ($\chi \rightarrow \chi \cdot N$). Therefore, any solution Φ_n of Eq.(1) with norm N is obtained from a solution Ψ_n with norm 1, through

$$\Phi_n(t; V, \chi) = \sqrt{N} \cdot \Psi_n(t; V, \chi N) \quad (4)$$

Furthermore, the magnitude of the hopping integral V can be considered unity by appropriate rescaling of time and χ . Changing sign in V is equivalent to the transformation $\Psi_n \rightarrow (-1)^n \Psi_n$ (or $\Psi_{n_x, n_y} \rightarrow (-1)^{n_x + n_y} \Psi_{n_x, n_y}$ in 2D, etc.). Therefore, in the following we consider $N = 1$ and $V = 1$ without loss of the generality, while the nonlinearity χ remains the only free parameter of the system.

1.1 Stationary solutions of DNLS

The stationary states of DNLS are characterized by a simple harmonic evolution with frequency ω :

$$\Psi_n = \psi_n \cdot e^{-i\omega t}. \quad (5)$$

The time independent amplitudes ψ_n satisfy the nonlinear eigenvalue problem

$$\omega\psi_n = -\sum_{\delta} \psi_{n+\delta} + \chi|\psi_n|^2\psi_n \quad (6)$$

(since we consider $V = 1$). The energy E_s of a stationary state is related to its frequency ω through

$$E_s = \omega - \frac{\chi}{2} \sum_n |\psi_n|^4. \quad (7)$$

There are two kinds of stationary solutions of Eq. (6): extended (like Bloch states and standing waves [22]) and localized states. The Bloch states, $\psi_n^q \sim \exp(iqn)$, form a band of frequencies or energies from $-2dV$ to $2dV$ (for an infinite d -dimensional lattice). Localized states have discrete frequencies outside of the Bloch band.

The most obvious and well studied localized state is the single-peaked solution, which has its maximum amplitude on one lattice site. This state has extreme (minimal for negative χ and maximal for positive χ) energy and frequency, compared to the other localized states. However, in general there are infinite (in an infinite lattice) multi-peaked stationary solutions of DNLS (which, for example, can be continued from trivial multi-peaked solutions of the anti-continuous limit), resulting in a very rich discrete spectrum with many quasi-degenerate levels (see below). In spite of this complexity, a part of the spectrum can be understood by classifying the stationary states from the anti-continuous limit. For the general concept of the anti-continuous, or anti-integrable, limit in nonlinear lattices see Ref. [23]. Here, multi-peaked and real stationary solutions of high symmetry, which have direct counterparts at the anti-continuous limit, are presented. Their location on the DNLS spectrum, their stability, and approximate analytical expressions are discussed.

2 Aubry's method for the numerical calculation of localized stationary states of DNLS

Localized stationary states can be obtained as attractors of the map:

$$\overline{\psi} \longrightarrow \overline{\psi'} = \text{sgn}\chi \cdot \frac{\Re\{\overline{\psi}\}}{\|\Re\{\overline{\psi}\}\|}. \quad (8)$$

In this equation, $\overline{\psi} = (\psi_1, \dots, \psi_L)$, where L is the total number of lattice sites, $\text{sgn}\chi$ denotes the sign of χ , $\Re\{\overline{\psi}\}$ is defined through the right-hand-side of the stationary equation (6), with its n -th component given by

$$\Re\{\overline{\psi}\}_n = - \sum_{\delta} \psi_{n+\delta} + \chi |\psi_n|^2 \psi_n, \quad (9)$$

and $\|\Re\{\overline{\psi}\}\|$ represents its norm $\sqrt{\sum_{n=1}^L |\Re\{\overline{\psi}\}_n|^2}$.

Starting the iterations from appropriate initial states, obtained through trivial solutions of the anti-continuous limit, i.e.

$$\psi_n^{(r=0)} = \delta_{n,n_0}, \quad \text{or} \quad \psi_n^{(r=0)} = \frac{1}{\sqrt{2}}(\delta_{n,n_0} \pm \delta_{n,n_1}), \quad \text{etc.}, \quad (10)$$

depending on the desired localized stationary solution (single-peaked, double-peaked with interpeak separation $|n_0 - n_1|$, etc.), and iteratively applying the map (8)

$$\psi_n^{(r+1)} = \text{sgn}\chi \cdot \frac{\Re\{\overline{\psi}^{(r)}\}_n}{\|\Re\{\overline{\psi}^{(r)}\}\|}, \quad (11)$$

the procedure can rapidly converge to the corresponding localized state.

Up to now this method has been successfully applied for calculating single-peaked stationary states of DNLS in 1D, 2D, and 3D [16], as well as for the single-peaked ground states in other similar systems [24,25,26,27,28]. The method has been invented by S. Aubry for finding polarons in the adiabatic Holstein model [29,30,31], a problem which reduces to the stationary solutions of DNLS.

In the following, after briefly recalling some results obtained in Ref [16] regarding the stable single-peaked stationary states of DNLS (section 3), this method is applied for calculating multi-peaked stationary solutions in 1D (section 4) and 2D (section 5). Stationary states are presented in sections 4 and

5 for negative values of χ ; the obtained solutions in this case can be directly transformed to the corresponding ones at $-\chi$ (i.e. at positive nonlinearities) by changing the sign of the frequency ($\omega \rightarrow -\omega$) and energy ($E_s \rightarrow -E_s$), and making the transformation $\psi_n \rightarrow (-1)^n \psi_n$ (or $\Psi_{n_x, n_y} \rightarrow (-1)^{n_x + n_y} \Psi_{n_x, n_y}$ in 2D, etc.) in the wavefunction. However, analytical results and the general discussion concern both signs of χ .

3 Single-peaked (SP) stationary states

For negative (positive) nonlinearity the single-peaked solution of DNLS corresponds to the lowest (highest) frequency stationary state. In 1D there is always a SP state with extreme frequency and energy, for any nonzero value of χ . As χ is approaching zero from negative (positive) values, the frequency and the energy of the SP solution tends to the bottom (top) of the Bloch band. The branch of SP solutions, as obtained by varying χ , has two well-known limits: for large $|\chi|$ (in the anti-continuous limit, where the first term of the right-hand-side of Eq. (6) can be neglected) tends to a single-site localized state ($\psi_n = \delta_{n, n_0}$), while for $|\chi| \rightarrow 0$ tends to a solution obtained by the soliton of the continuous nonlinear Schrödinger equation (see Eq. (14) below).

The picture is qualitatively different in 2D and 3D. In these cases there is a critical value of nonlinearity $\chi_1 > 0$, such that for $|\chi| < \chi_1$ does not exist a single-peaked, or any other localized, stationary state. At $|\chi| = \chi_1$ a pair of SP states appears, through a saddle-node bifurcation; a narrow stable solution of high amplitude and an unstable one of relatively large extent and small amplitude. Due to the simultaneous existence of two SP states and the proximity of the unstable one with the extended Bloch states of the band edges, it is not paid any attention to the unstable solution and from now on we exclusively refer to the stable one wherever a single-peaked state is mentioned in 2D or 3D. A second nonlinearity threshold $\chi_2 > \chi_1$ exists, such that for $\chi_1 < |\chi| < \chi_2$ the SP state has extreme frequency, but not extreme energy, since its energy E_s lies inside the Bloch band. Only for $|\chi| > \chi_2$ the single-peaked stationary solution provides an extreme of the energy (i.e. it is the ground state for negative χ). In 2D the values of these thresholds are $\chi_1 \approx 5.701$ and $\chi_2 \approx 6.679$, while in 3D are $\chi_1 \approx 7.852$ and $\chi_2 \approx 10.816$ [16]¹.

Analytical approximate expressions have been presented in Ref. [16], which accurately describe the SP stationary states. In particular, for the whole branch of SP solutions in 2D and 3D, as well as for values of $|\chi|$ larger than about 3

¹ Note that the nonlinear parameter χ used in this work corresponds to $-k^2$ of Ref. [16].

in 1D, the exponentially decaying function

$$\psi_{n_x, n_y, n_z}^{SP} = \left(\frac{1 - \zeta^2}{1 + \zeta^2} \right)^{d/2} \cdot \zeta^{|n_x| + |n_y| + |n_z|}, \quad \text{with } \zeta = -\frac{1}{\chi} - \frac{4d - 2}{\chi^3} \quad (12)$$

(where one has to disregard the index n_z in 2D and both n_z and n_y in 1D), can be used to describe the exact SP solution. The corresponding frequencies and energies are given by

$$\omega = \chi - \frac{2d(4d - 3)}{\chi^3} \quad \text{and} \quad E_s = \frac{\chi}{2} + \frac{2d}{\chi} + \frac{d(4d - 3)}{\chi^3}. \quad (13)$$

The expression (12) is derived from a variational method, by employing a perturbative expansion of ζ in powers of $1/\chi$ in the condition providing the minima of the variational energy. The next non-zero correction of ζ in Eq.(12) is of the order of $1/\chi^5$.

The above analytical results describe accurately (the larger the $|\chi|$ the better the approximation) the SP solutions of DNLS in all cases, except for relatively small values of $|\chi|$ in 1D. Then a smooth transition occurs for $|\chi|$ in the region $2.5 - 3$, from the above expressions to the static soliton of the continuous nonlinear Schrödinger equation. Therefore, for $|\chi|$ smaller than about 2.5 the SP solutions in 1D can be approximated by

$$\psi_n^{SP} = (-sgn\chi)^n \sqrt{\frac{|\chi|}{8}} \cdot \frac{1}{\cosh \frac{\chi n}{4}}, \quad (14)$$

with corresponding frequency and energy

$$\omega = sgn\chi \cdot \left(2 + \frac{\chi^2}{16} \right) \quad \text{and} \quad E_s = sgn\chi \cdot \left(2 + \frac{\chi^2}{48} \right). \quad (15)$$

Note that the $(-sgn\chi)^n$ term in (14) provides the alteration of signs in successive lattice sites, which characterizes the solution at positive χ . In Eq. (12) this is obtained through the negative sign of ζ .

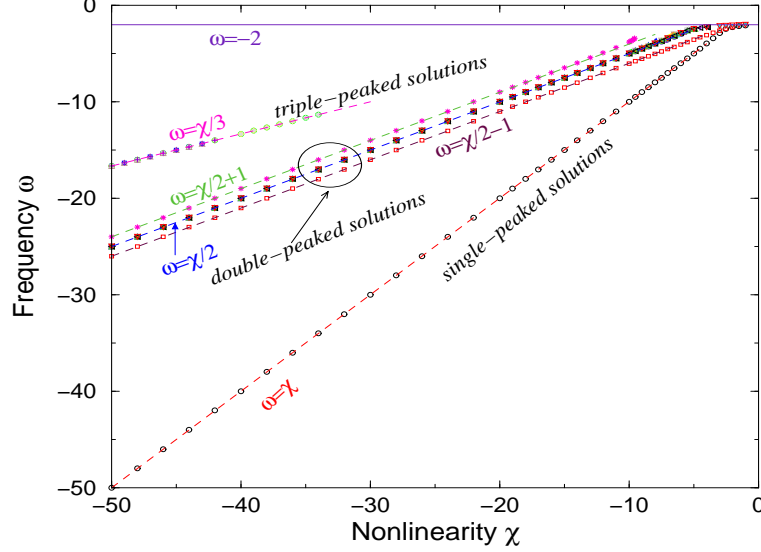


Fig. 1. Frequencies of single- double- and triple-peaked stationary solutions of DNLS in 1D (points). Dashed lines show analytical expressions obtained for large values of $|\chi|$. The horizontal line at $\omega = -2$ indicates the lower edge of the band of Bloch stationary states, which extends from -2 to 2 . The spectrum is antisymmetric on χ ; $\omega(-\chi) = -\omega(\chi)$.

4 Multi-peaked solutions in 1D

4.1 Frequency spectrum

As it has been already mentioned in the introduction, the frequency (or energy) spectrum of DNLS in 1D comprises many discrete levels, corresponding to single-peaked and multi-peaked localized stationary solutions.

These discrete levels have well determined limits in the anti-continuous regime. In this limit the discrete spectrum is given by

$$\omega = \frac{\chi}{M}, \quad E_s = \frac{\chi}{2M}, \quad \text{where } M = 1, 2, 3, \dots \quad (16)$$

Each (highly degenerate) level of Eq.(16) corresponds to any M -peaked stationary state, where all the M peaks (at arbitrary sites) have the same norm $1/\sqrt{M}$ (and arbitrary complex phases). Such stationary solutions can be continued away from the anti-continuous limit [30] up to some value of χ , depending on the particular state.

A stationary solution at a given value of χ is classified as a single- double- or, in general, M -peaked state, depending on how many sites (one, two, or in general M , respectively) are occupied at the anti-continuous limit of the branch in

which this state belongs. Such a classification is always possible for stationary states of high symmetry. Moreover, it can be used for *each* stationary solution, providing a complete description of the discrete spectrum, up to $\omega \approx -5.45$ [32].

Fig. 1 shows a part of the frequency spectrum which contains contributions from many double-peaked solutions, as well as few branches (just shown for indication) of triple-peaked states. Analytical expressions, obtained at large values of $|\chi|$ and shown by dashed lines, describe well these branches (the next corrections are of the order of inverse powers of χ , see Appendix). Bifurcations lead to the disappearance of some branches (or merging with other branches) by decreasing the strength of nonlinearity.

What appears as a middle branch of the double-peaked (DP) solutions in Fig. 1 actually consists of many branches of closely spaced levels (corresponding to DP solutions with any interpeak separation larger than one lattice constant), which merge to the level of Eq.(16) for $M = 2$ as $|\chi|$ increases. The lower and upper branch of the DP solutions are single branches corresponding to symmetric and antisymmetric, respectively, double-peaked states with their peaks at neighboring lattice sites (examples are shown at the upper left plots of Figs. 2 and 3, respectively). The interpeak separation of a DP state is determined by the distance S of the sites where the peaks appear. Symmetric and antisymmetric DP solutions in 1D, with various interpeak distances, are presented in the following subsection.

4.2 Double-peaked symmetric and antisymmetric solutions

4.2.1 Stationary states

In order to find the branches of symmetric and antisymmetric DP solutions, the method described in section 2 is applied using as initial states

$$\psi_n^{(r=0)} = \frac{1}{\sqrt{2}}(\delta_{n,n_1} + \delta_{n,n_2}) \quad \text{and} \quad \psi_n^{(r=0)} = \frac{1}{\sqrt{2}}(\delta_{n,n_1} - \delta_{n,n_2}), \quad (17)$$

respectively. The distance $|n_2 - n_1|$ determines the interpeak separation S of the corresponding solution.

Stationary solutions with interpeak separations 1, 2, 10, and 20 sites are shown for different values of χ in Fig. 2 for symmetric and in Fig. 3 for antisymmetric states. As it is expected, by decreasing $|\chi|$ the solutions spread more and more, until a value of χ where a bifurcation occurs resulting in the disappearance of the corresponding branch. The smaller values of $|\chi|$ shown at each plot of Fig. 2 (apart from the case of $S = 1$, displayed in Fig. 2a) and Fig. 3

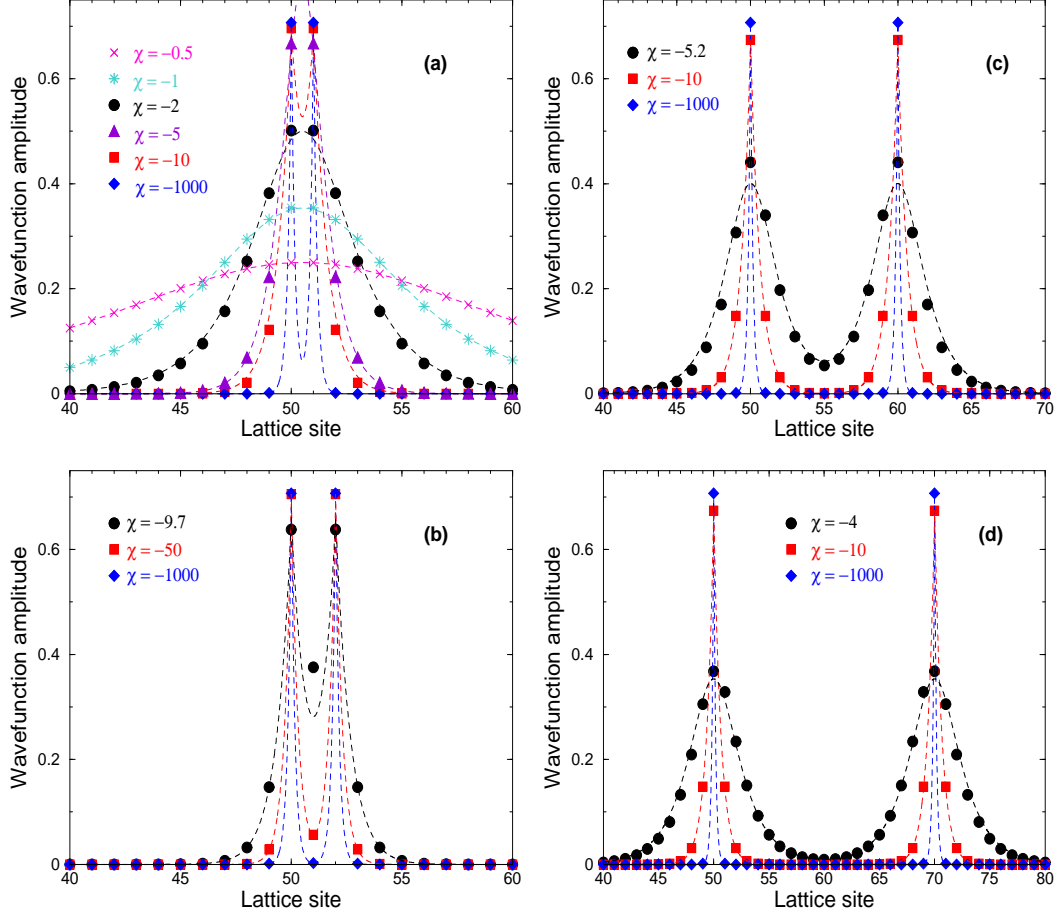


Fig. 2. Double-peaked symmetric stationary solutions of DNLS in 1D (points) for different values of the nonlinearity χ and various interpeak separations S : (a) $S = 1$ lattice site, (b) $S = 2$ sites, (c) $S = 10$ sites, and (d) $S = 20$ sites. Dashed lines show analytical approximations of the solutions using Eq. (18) for the discrete cases where $|\chi| > 6$, Eq. (21) for $\chi = -5.2$ in (c) and $\chi = -4$ in (d), and Eq. (14) centered in the middle between the sites of maximum amplitude for $\chi = -0.5$ up to -5 in (a) (see text).

are close to the bifurcation point and therefore represent one of the most extended solutions of the corresponding branch. The case of symmetric states with interpeak distance equal to one lattice constant (Fig. 2a) is exceptional in this respect, since the corresponding branch survives until the limit $|\chi| \rightarrow 0$, as it merges to the SP branch for sufficiently small values of $|\chi|$. As the continuous limit is approached, the DP symmetric state with $S = 1$ becomes practically indistinguishable from the SP state, i.e. the solution given by Eq. (14).

The symmetric (antisymmetric) states with $S = 1$ provide the lower (upper) single branch of the DP solutions of Fig. 1, with frequency equal to $\omega = \frac{\chi}{2} - 1$ ($\omega = \frac{\chi}{2} + 1$), for relatively large $|\chi|$. All the other symmetric and antisymmetric DP solutions with interpeak separations $S > 1$ are congested in the middle branch (with frequency equal to $\omega = \frac{\chi}{2}$ for large $|\chi|$). In particular, in Fig. 1

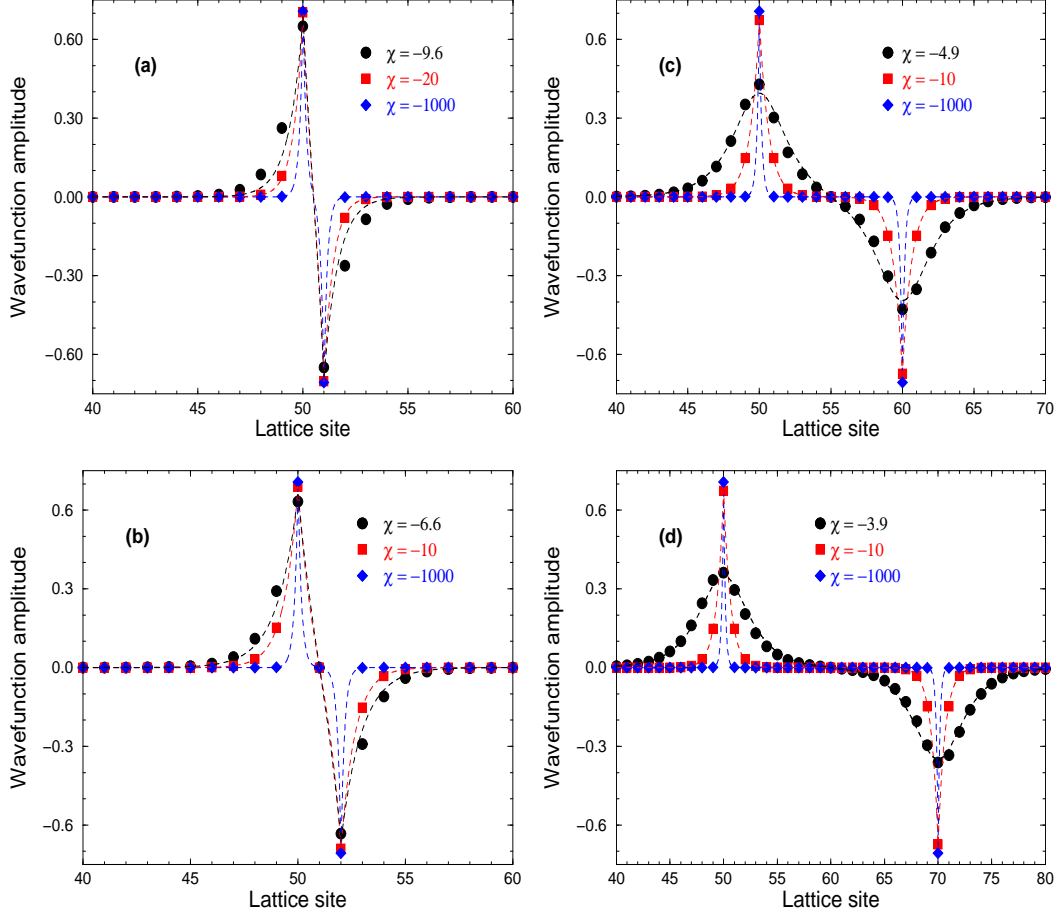


Fig. 3. Double-peaked antisymmetric stationary solutions of DNLS in 1D (points) for different values of the nonlinearity χ and various interpeak separations S : (a) $S = 1$ lattice site, (b) $S = 2$ sites, (c) $S = 10$ sites, and (d) $S = 20$ sites. Dashed lines show analytical approximations of the solutions using Eq. (18) in the discrete cases where $|\chi| > 6$ and Eq. (21) in the two more extended cases of (c) and (d).

the middle branch contains solutions for $S = 2, 3, 4, 5, 10, 20$, and 200 . As the interpeak separation S increases, the two peaks start to not overlap much, even for small values of $|\chi|$, and in this case the corresponding branch survives longer (i.e. persists closer to $\chi = 0$). These branches, as $|\chi|$ decreases, eventually deviate from the line $\omega = \frac{\chi}{2}$, and for even smaller values of $|\chi|$ they can be described by double-peaked solutions of the continuous nonlinear Schrödinger equation.

Approximate analytical expressions, which describe the DP states in the most of the cases, can be obtained by appropriate superpositions of the single-peaked states (12) and (14). One has to take into account that when the two peaks do not significantly overlap the norm of each peak is about half of the total norm. Then from Eq. (4) follows that the two individual wavefunctions superimposed in a double-peaked solution should be provided by Eqs. (12)

or (14) corresponding to $\frac{\chi}{2}$. As a result a symmetric or antisymmetric DP solution with interpeak separation S , where the first peak is located at the site n_1 and the second at $n_2 = n_1 + S$ (S is assumed to be positive), can be approximated by

$$\psi_n^{DP} = \frac{1}{\sqrt{2(1 \pm P)}} \sqrt{\frac{1 - \zeta^2}{1 + \zeta^2}} \left(\zeta^{|n-n_1|} \pm (-\text{sgn}\chi)^S \zeta^{|n-n_1-S|} \right), \quad (18)$$

$$\text{where } P = (-\text{sgn}\chi)^S \frac{(1+S)\zeta^S - (S-1)\zeta^{S+2}}{1 + \zeta^2} \quad (19)$$

$$\text{and } \zeta = -\frac{1}{\chi/2} - \frac{2}{(\chi/2)^3} = -\frac{2}{\chi} - \frac{16}{\chi^3}, \quad (20)$$

or

$$\psi_n^{DP} = \frac{(-\text{sgn}\chi)^{n-n_1}}{\sqrt{2(1 \pm P)}} \sqrt{\frac{|\chi|}{16}} \left(\frac{1}{\cosh \frac{\chi(n-n_1)}{8}} \pm \frac{(-\text{sgn}\chi)^S}{\cosh \frac{\chi(n-n_1-S)}{8}} \right), \quad (21)$$

$$\text{where } P = (-\text{sgn}\chi)^S \frac{\frac{\chi S}{8}}{\sinh \frac{\chi S}{8}}. \quad (22)$$

The former (latter) solution can be used for a DP state with discrete (rather extended) peaks, valid for relatively large (small) values of $|\chi|$. Roughly speaking the transition from one form to the other occurs for $|\chi|$ in the region 5–6. The normalization factors P in Eqs. (19) and (22) result from the non-orthogonality of the superimposed wavefunctions, i.e. $P = \sum_n \psi_n^{SP[n_1]}(\frac{\chi}{2}) \psi_n^{SP[n_1+S]}(\frac{\chi}{2})$, where $\psi_n^{SP[m]}(\frac{\chi}{2})$ denotes the SP solution centered at the site m and calculated for the value $\frac{\chi}{2}$ of the nonlinearity parameter. The plus (minus) signs in these approximate solutions correspond to symmetric (antisymmetric) states, except for the case of positive χ and odd S , where they give the antisymmetric (symmetric) DP state.

Eq. (21) is not applicable for small values of $|\chi|$ in the exceptional case of symmetric states with $S = 1$, due to the significant overlap of the two non-distinguished peaks (Fig. 2a for $|\chi|$ approximately less than 5-6). In this case the corresponding DP solution, whose branch is merging to the single-peaked branch, can be well described by Eq. (14) centered in the middle between the consecutive sites of the two peaks. The analytical approximations discussed above have been plotted in Figs. 2 and 3 (dashed lines) along with the numerical solutions (points) for comparison. In particular, Eq. (14) has been used, as just explained, in Fig. 2a for $\chi = -0.5, -1, -2$, and -5 , Eq. (21) has been used only for the smallest values of $|\chi|$ in Figs. 2c, 2d, 3c, and 3d (where $|\chi| < 6$), and Eq. (18) has been plotted in all the other cases. The

more distinguished the two peaks, i.e. the higher the S , or the higher the $|\chi|$ even for smaller values of S , the better the approximations (18) and (21) are.

4.2.2 Linear stability

Symmetric and antisymmetric DP states show qualitatively different behavior regarding their stability. A detailed investigation of the stability eigenvalues is presented below for negative values of χ . From this, the behavior at positive χ can be obtained as follows: for even S the situation, regarding the stability eigenvalues, is exactly the same as that of $\chi < 0$, while for odd S the symmetric (antisymmetric) states behave exactly like the antisymmetric (symmetric) states of $\chi < 0$. Note here that the transformation $(-1)^n \psi_n$, connecting stationary solutions at opposite values of χ , turns a symmetric DP state to antisymmetric and vis versa when S is odd. Therefore, what is mentioned below for $\chi < 0$, also holds as it is for $\chi > 0$ when S is even, while it holds after interchanging roles between symmetric and antisymmetric states when S is odd.

The eigenvalues of the linear stability problem are always obtained as pairs of opposite sign and there always exists a pair of eigenvalues at zero. In our approach (see Appendix), if there is an eigenvalue with non-zero imaginary part, then the stationary solution is unstable. All relevant discussions in this and the following section will refer to those eigenvalues with non-negative real part, without usually mentioning the pinned pair of eigenvalues at zero. The spectrum of eigenvalues is always symmetric with respect to the imaginary axis. The complete structure of the linear stability spectrum close to the anti-continuous limit is analytically derived in the Appendix.

For negative χ , the nonlinear term of DNLS has the same sign as the tunneling term. Then it is known that the symmetric DP states are unstable [33,34], in contrary to the case of the antisymmetric ones that may be linearly stable [4,35]. In fact, the latter are linearly stable in the larger part of the corresponding branch. When this branch becomes unstable, by decreasing $|\chi|$, soon it disappears. The larger the interpeak distance, the smaller the $|\chi|$'s at which the branch turns unstable and disappears. The scenario for development of instability and disappearance seems to roughly be as follows. For large $|\chi|$, linear stability analysis provides, a discrete eigenvalue outside of the band. For relatively large $|\chi|$ the band extends from $\frac{|\chi|}{2} - 2$ to $\frac{|\chi|}{2} + 2$, apart from the case of symmetric (antisymmetric) states with interpeak separation $S = 1$, where it extends from $\frac{|\chi|}{2} - 1$ to $\frac{|\chi|}{2} + 3$ (from $\frac{|\chi|}{2} - 3$ to $\frac{|\chi|}{2} + 1$). As $|\chi|$ decreases, the band moves towards zero, while the discrete eigenvalue keeps off zero for $S > 2$, remains almost constant for $S = 2$, and goes to zero (but slower than the band) for $S = 1$. After their collision (or the collision of the discrete eigenvalue with another eigenvalue splitted off the band) the insta-

Table 1

Nonlinearity strength χ for the development of instability and disappearance of antisymmetric and the disappearance of symmetric double-peaked stationary solutions of DNLS at different interpeak separations. Values in parentheses in the second column show rough analytical estimates using Eq. (24).

Interpeak separation	Regime of χ at which the antisymmetric branch becomes unstable	Regime of χ at which the antisymmetric branch disappears	Regime of χ at which the symmetric branch disappears
$S = 1$	$[-19.73, -19.72] \quad (-18)$	$[-9.58, -9.57]$	—
$S = 2$	$[-8.8, -8.7] \quad (-8)$	$[-6.54, -6.53]$	$[-9.63, -9.62]$
$S = 3$	$[-7.1, -7.0] \quad (-6.3)$	$[-5.9, -5.8]$	$[-7.9, -7.8]$
$S = 4$	$[-6.5, -6.4] \quad (-5.5)$	$[-5.7, -5.6]$	$[-7.0, -6.9]$
$S = 5$	$[-6.2, -6.1] \quad (-5.0)$	$[-5.5, -5.4]$	$[-6.5, -6.4]$
$S = 10$	$[-5.0, -4.9] \quad (-4.2)$	$[-4.9, -4.8]$	$[-5.2, -5.1]$
$S = 20$	$[-3.90, -3.89] \quad (-4.0)$	$[-3.90, -3.89]$	$[-4.0, -3.9]$

bility develops. As $|\chi|$ decreases more, the band is approaching zero and the branch disappears when an eigenvalue splitted from the band collides with the pinned eigenvalue at zero. Table 1 shows for antisymmetric DP solutions of various interpeak separations (first column) the nonlinearity regime where the corresponding branch becomes unstable (second column; for larger values of $|\chi|$ the solutions are linearly stable) and the nonlinearity regime where the branch disappears (third column).

Regarding the unstable symmetric DP states, linear stability analysis reveals that there is always one pair of purely imaginary unstable eigenvalues. If the magnitude of instability is denoted by λ_u (i.e. the unstable eigenvalues are $\pm i\lambda_u$), then for fixed value of χ , λ_u decreases as the interpeak separation increases. For fixed interpeak distance S , but larger than two lattice sites, λ_u decreases by increasing $|\chi|$. For $S = 2$, λ_u tends to a constant value for large $|\chi|$, while for $S = 1$, λ_u decreases with decreasing $|\chi|$, in accordance with the fact that this branch merges to the stable single-peaked branch for $|\chi| \rightarrow 0$. This behavior is shown in Fig. 4. In some cases, especially for large interpeak separations, the magnitude of instability is so small that for any practical purpose the corresponding solution can be considered as quasi-stable [33]. The log-log plot of λ_u as a function of $|\chi|$ in Fig. 4 demonstrates a power-law dependence $\lambda_u \sim |\chi|^a$ at large values of $|\chi|$. Relating the stability eigenvalues with the energy spectrum of a tight-binding problem in the presence of a deep and narrow double-well potential (see Appendix), one obtains

$$\lambda_u = 2^{S/2} |\chi|^{1-\frac{S}{2}}, \quad \text{for } |\chi| \gg 1. \quad (23)$$

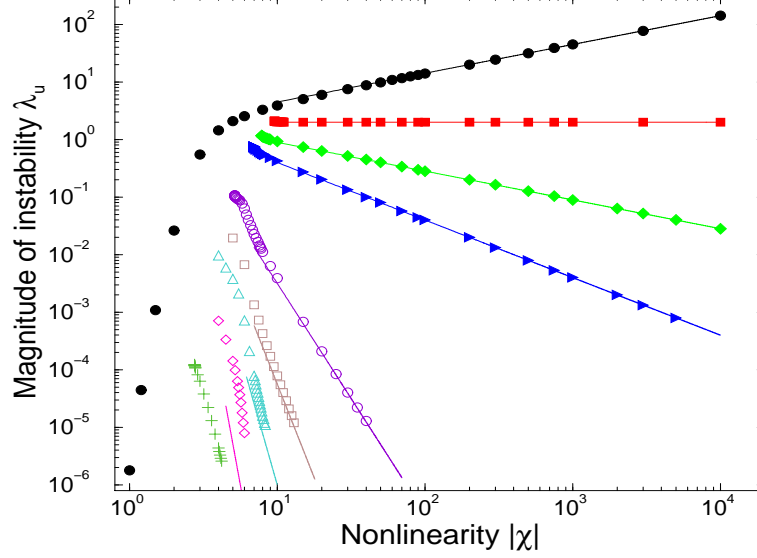


Fig. 4. Magnitude of instability λ_u of symmetric double-peaked solutions of DNLS for $\chi < 0$ in 1D (points) as a function of the strength of nonlinearity $|\chi|$, for various interpeak separations: $S = 1$ (filled circles), $S = 2$ (filled squares), $S = 3$ (filled diamonds), $S = 4$ (filled triangles), $S = 10$ (open circles), $S = 15$ (open squares), $S = 20$ (open triangles), $S = 30$ (open diamonds), and $S = 50$ (crosses). Lines show the power-law relation, Eq.(23), derived for relatively large values of $|\chi|$.

This relation is plotted in Fig. 4 for $S = 1, 2, 3, 4, 10, 15, 20$, and 30 (solid lines) along with the corresponding numerical results (points). The agreement is very good for $|\chi|$ larger than $10 - 20$.

The disappearance of the symmetric branches occurs for non-zero χ (apart from the case of $S = 1$, where the corresponding branch merges with the SP branch) when, as in the antisymmetric case, a real eigenvalue splitted from the band collides with the pinned eigenvalues at zero. Table 1 shows (fourth column) the nonlinearity regime where different branches of symmetric DP solutions disappear. It seems that for fixed S ($S > 1$), the antisymmetric branches survive until smaller values of $|\chi|$.

As it is shown in the Appendix, close to the anti-continuous limit the stable (real) discrete eigenvalue of an antisymmetric DP state has the same dependence like in Eq. (23) (see Eq. (52)). Numerical simulations confirm that for relative large $|\chi|$ the stable eigenvalues of antisymmetric states have the same magnitude with the unstable of the symmetric ones. This result can be used for a rough estimate of the nonlinearity value, χ_{un} , where an antisymmetric state becomes unstable (through the collision of the discrete eigenvalue with the band), by

$$\frac{|\chi|}{2} - 2 = 2^{S/2} |\chi|^{1-\frac{S}{2}} \quad \text{for } S > 1, \quad \text{or} \quad \frac{|\chi|}{2} - 3 = \sqrt{2|\chi|} \quad \text{for } S = 1, \quad (24)$$

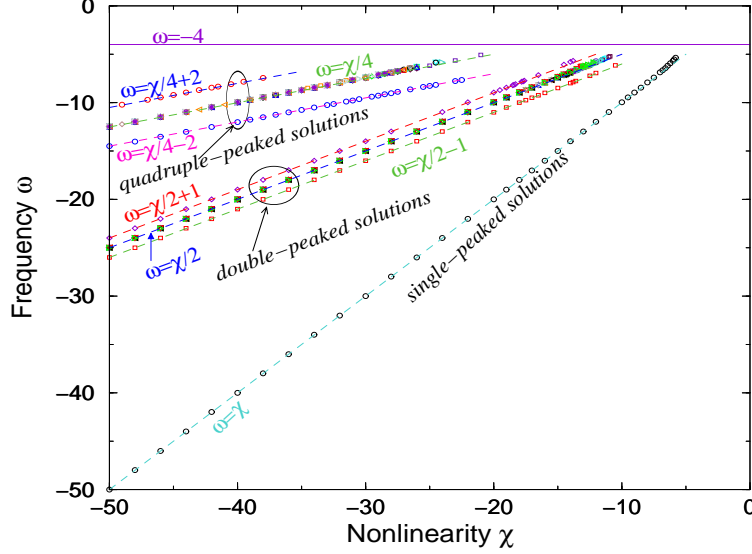


Fig. 5. Frequencies of single- double- and quadruple-peaked stationary solutions of DNLS in 2D (points). Dashed lines show analytical expressions obtained for large values of $|\chi|$. The horizontal line at $\omega = -4$ indicates the lower edge of the band of Bloch stationary states, which extends from -4 to 4 . The spectrum is antisymmetric on χ ; $\omega(-\chi) = -\omega(\chi)$.

where $\frac{|\chi|}{2} - 2$ ($\frac{|\chi|}{2} - 3$) is the lower band edge. The larger the $|\chi_{un}|$ the better the estimate, since Eq. (23) is valid for $|\chi| \gg 1$. Estimates of χ_{un} , resulting from the solution of Eq. (24), are shown in the second column of Table 1 inside parentheses, next to the numerical results. The relative error is less than 10% for $S = 1$ and $S = 2$, but it increases for larger S where $|\chi_{un}|$ is getting smaller.

5 Multi-peaked solutions in 2D

5.1 Frequency spectrum

Similarly to the 1D case, also in 2D there are many families of multi-peaked localized stationary states corresponding to discrete levels in the frequency spectrum. For large values of $|\chi|$ these levels tend to the anti-continuous limit spectrum. Fig. 5 shows a part of the frequency spectrum in 2D, which, apart from the single-peaked states of lowest frequency, contains many branches of double-peaked and quadruple-peaked (QP) stationary solutions at various interpeak distances.

All the calculated DP states (symmetric or antisymmetric, along the lattice axes or along the diagonal, and with different interpeak separations) have

frequencies around $\omega = \frac{\chi}{2}$, apart from the symmetric and antisymmetric states with their two peaks at neighboring sites (examples are shown at the left columns of Fig. 6 and Fig. 7), which have frequencies around $\omega = \frac{\chi}{2} - 1$ and $\omega = \frac{\chi}{2} + 1$, respectively. Therefore, from the branches of the DP solutions of Fig. 5, the middle one is highly crowded, tending to the level of Eq.(16) for $M = 2$ at large $|\chi|$, while the two external branches are single branches.

Similar considerations are valid for the branches of quadruplet stationary states. What appears as a middle branch of the QP states in Fig. 5 actually contains many stationary solutions with frequencies around $\omega = \frac{\chi}{4}$. Below and above these highly congested branches there are single branches corresponding to the symmetric (see left column of Fig. 10) and antisymmetric (see left column of Fig. 11) solutions, respectively, with their four peaks on the corners of the unit cell of the square lattice.

Multi-peaked stationary states, representative of some of the branches shown in Fig. 5, are presented in the following two subsections and their linear stability is discussed. Note that there also exist triple-peaked solutions (with their positive or negative peaks along the axes, or along the diagonal, or at random sites), which are not discussed here. Only to mention that their corresponding branches tend to $\omega = \frac{\chi}{3}$ for large values of $|\chi|$, i.e. are in between the double-peaked and quadruple-peaked branches shown in Fig. 5.

5.2 Double-peaked solutions

DP solutions with the two peaks along a lattice axis (let say the y-axis) are presented first. The corresponding branches are calculated starting from the initial state

$$\psi_{n_x, n_y}^{(r=0)} = \frac{1}{\sqrt{2}}(\delta_{n_x, n_1} \delta_{n_y, n_2} + \delta_{n_x, n_1} \delta_{n_y, n_2+S}) \quad (25)$$

for the symmetric and

$$\psi_{n_x, n_y}^{(r=0)} = \frac{1}{\sqrt{2}}(\delta_{n_x, n_1} \delta_{n_y, n_2} - \delta_{n_x, n_1} \delta_{n_y, n_2+S}) \quad (26)$$

for the antisymmetric stationary states, respectively, where $S = 1, 2, \dots$ determines the interpeak separation along the lattice axis. Figs. 6 and 7 show examples for $S = 1$ (left columns), $S = 2$ (middle columns), and $S = 3$ (right columns). Fig. 5 contains branches of such solutions for $S = 1, 2, 3, 4, 5$, and 10. For $S = 1$ the upper and lower single branches of the DP states of Fig. 5 are obtained.

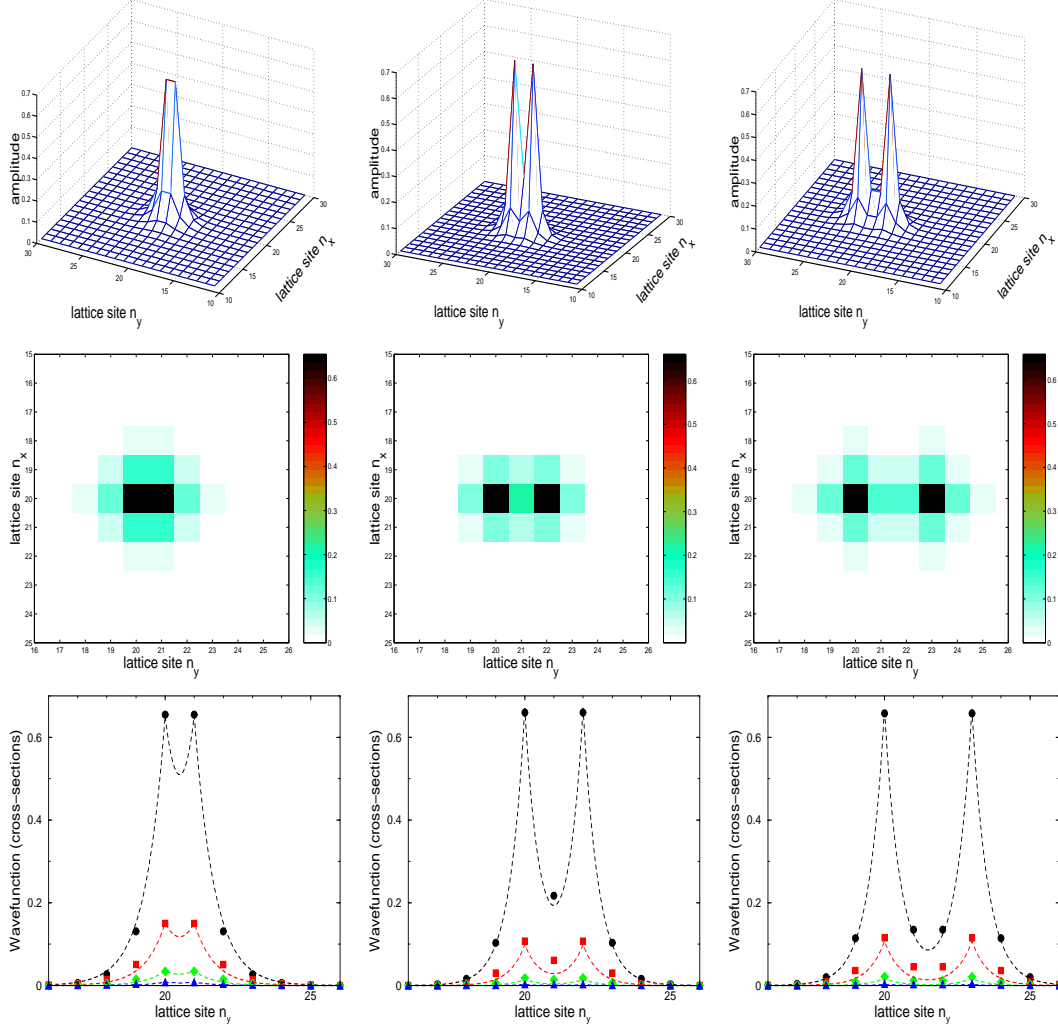


Fig. 6. 3D plots (first row) and density plots (second row) of double-peaked symmetric solutions (with their peaks along a lattice axis) of DNLS in 2D. *Left column*: interpeak separation $S = 1$ lattice site, $\chi = -10.5$. *Middle column*: interpeak separation $S = 2$ sites, $\chi = -15$. *Right column*: interpeak separation $S = 3$ sites, $\chi = -14$. Cross-sections of the wavefunctions are shown in the third row with points: $\psi_{n_x=n_1, n_y}$ (filled circles), $\psi_{n_x=n_1+1, n_y}$ (filled squares), $\psi_{n_x=n_1+2, n_y}$ (filled diamonds), $\psi_{n_x=n_1+3, n_y}$ (filled triangles), where $n_1 = 20$ is the x -coordinate of the two peaks. Dashed lines show analytical approximations of the solutions using Eq. (29).

Branches of DP solutions with their two peaks along the diagonal of the lattice axes have been also shown in Fig. 5. These branches are obtained starting from the initial state

$$\psi_{n_x, n_y}^{(r=0)} = \frac{1}{\sqrt{2}} (\delta_{n_x, n_1} \delta_{n_y, n_2} \pm \delta_{n_x, n_1+l} \delta_{n_y, n_2+l}), \quad (27)$$

where the plus sign gives the symmetric and the minus the antisymmetric, respectively, stationary states. Fig. 5 contains branches of these solutions for

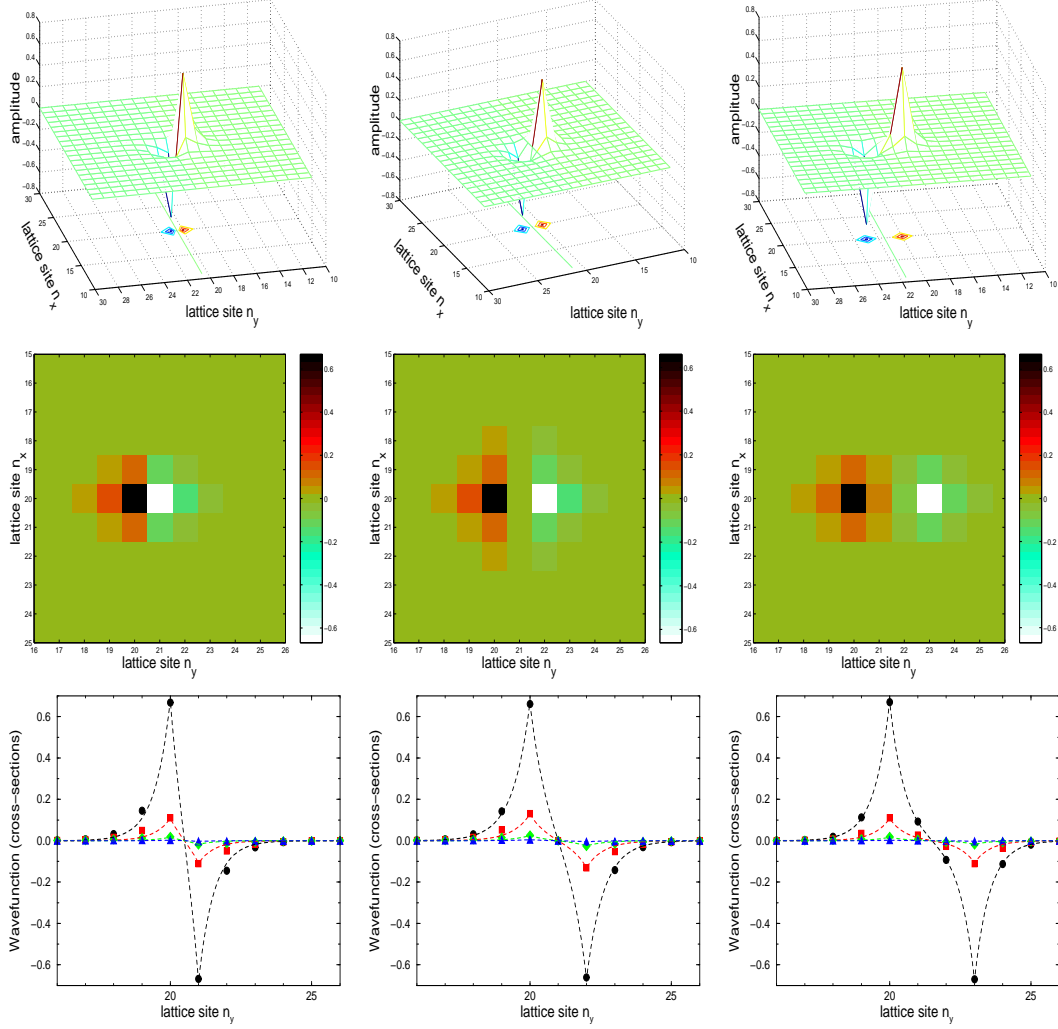


Fig. 7. 3D plots (first row) and density plots (second row) of double-peaked antisymmetric solutions (with their peaks along a lattice axis) of DNLS in 2D. *Left column:* interpeak separation $S = 1$ lattice site, $\chi = -14$. *Middle column:* interpeak separation $S = 2$ sites, $\chi = -12$. *Right column:* interpeak separation $S = 3$ sites, $\chi = -14$. Cross-sections of the wavefunctions are shown in the third row with points: $\psi_{n_x=n_1, n_y}$ (filled circles), $\psi_{n_x=n_1+1, n_y}$ (filled squares), $\psi_{n_x=n_1+2, n_y}$ (filled diamonds), $\psi_{n_x=n_1+3, n_y}$ (filled triangles), where $n_1 = 20$ is the x -coordinate of the two peaks. Dashed lines show analytical approximations of the solutions using Eq. (29).

$l = 1, 2, 3$, and 10 and their frequencies are around $\omega = \frac{\chi}{2}$. Some examples of such states are shown in Fig. 8.

Finally, many other DP solutions exist, with their peaks, of the same or opposite sign, at random lattice sites (not aligned along a lattice axis, or the diagonal). These can be obtained starting from the initial state

$$\psi_{n_x, n_y}^{(r=0)} = \frac{1}{\sqrt{2}} (\delta_{n_x, n_1} \delta_{n_y, n_2} \pm \delta_{n_x, n_1+S_x} \delta_{n_y, n_2+S_y}), \quad (28)$$

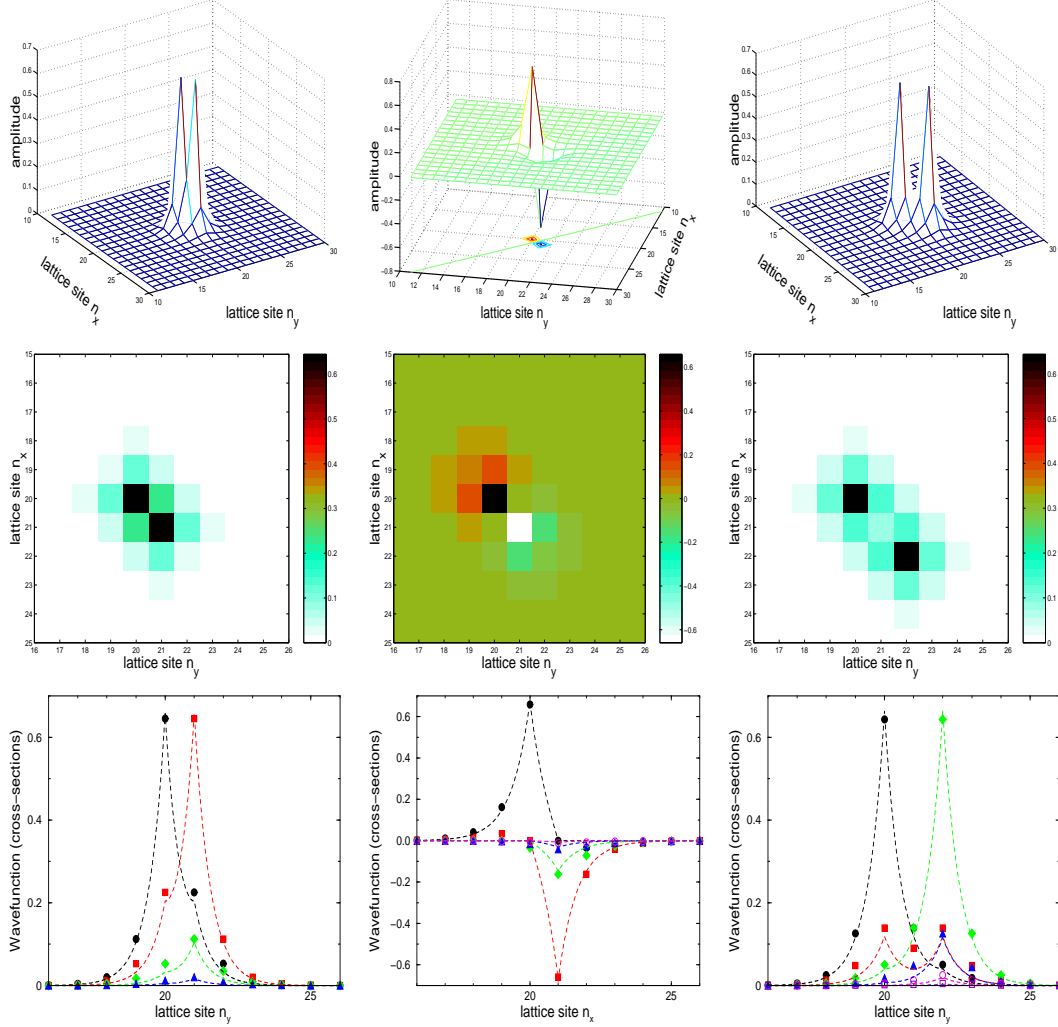


Fig. 8. 3D plots (first row) and density plots (second row) of double-peaked symmetric and antisymmetric solutions (with their peaks along the diagonal of the lattice axes) of DNLS in 2D. *Left column:* symmetric state with $l = 1$ and $\chi = -14.1$. *Middle column:* antisymmetric state with $l = 1$ and $\chi = -11$. *Right column:* symmetric state with $l = 2$ and $\chi = -13.1$. Cross-sections of the wavefunctions are shown in the third row with points: $\psi_{n_x=n_1, n_y}$ (filled circles), $\psi_{n_x=n_1+1, n_y}$ (filled squares), $\psi_{n_x=n_1+2, n_y}$ (filled diamonds), $\psi_{n_x=n_1+3, n_y}$ (filled triangles), $\psi_{n_x=n_1+4, n_y}$ (open circles, in the second and third column), $\psi_{n_x=n_1+5, n_y}$ (open squares, in the third column), where $n_1 = 20$ is the x-coordinate of the first peak. Dashed lines show analytical approximations of the solutions using Eq. (29).

with any combination of non-zero integers S_x , S_y and $S_x \neq S_y$. The corresponding branches are close to the middle branch of the DP solutions of Fig. 5.

As in the 1D case, one can obtain approximate analytical expressions for the DP solutions of DNLS in 2D, by appropriate superpositions of the single-peaked solutions (12). If (n_1, n_2) is the lattice site of the first peak and $(n_1 +$

$S_x, n_2 + S_y$) of the second one (S_x and S_y are assumed to be positive), then the corresponding approximate solution is

$$\psi_{n_x, n_y}^{DP} = \frac{1}{\sqrt{2(1 \pm P)}} \frac{1 - \zeta^2}{1 + \zeta^2} \left(\zeta^{|n_x - n_1| + |n_y - n_2|} \pm (-\text{sgn}\chi)^{S_x + S_y} \zeta^{|n_x - n_1 - S_x| + |n_y - n_2 - S_y|} \right), \quad (29)$$

$$\text{where } P = (-\text{sgn}\chi)^{S_x + S_y} \frac{[(1 + S_x) - (S_x - 1)\zeta^2][(1 + S_y) - (S_y - 1)\zeta^2]\zeta^{S_x + S_y}}{(1 + \zeta^2)^2} \quad (30)$$

$$\text{and } \zeta = -\frac{1}{\chi/2} - \frac{6}{(\chi/2)^3} = -\frac{2}{\chi} - \frac{48}{\chi^3}. \quad (31)$$

Here also, the individual wavefunctions superimposed in this solution should correspond to $\frac{\chi}{2}$, which has been taken into account in the relation (31) providing ζ . The plus and minus signs in Eq. (29) correspond to symmetric and antisymmetric states, respectively, apart from the case of positive χ and odd S where it is the other way around. The overlap P of the two superimposed single-peaked solutions is $P = \sum_{n_x, n_y} \psi_{n_x, n_y}^{SP[n_1, n_2]}(\frac{\chi}{2}) \psi_{n_x, n_y}^{SP[n_1 + S_x, n_2 + S_y]}(\frac{\chi}{2})$, where $\psi_{n_x, n_y}^{SP[n_1, n_2]}(\frac{\chi}{2})$ is the SP solution in 2D, centered at (n_1, n_2) and corresponding to $\frac{\chi}{2}$. Cross-sections of the approximate solution (29) are shown with dashed lines in the third rows of Figs. 6-8.

Concerning the stability of the DP stationary states, the picture is similar like in 1D. For $\chi < 0$, or $\chi > 0$ and even S , all the symmetric solutions are unstable, while the antisymmetric ones are in general (at least for relatively large values of $|\chi|$) linearly stable. For $\chi > 0$ and odd S the reverse is true. General arguments are presented in the Appendix showing that close to the anti-continuous limit any symmetric (antisymmetric) DP solution should be unstable (linearly stable), except when $\chi > 0$ and S is odd, where it is linearly stable (unstable). Further, this calculation allows to determine the variation of the magnitude of instability λ_u of the unstable solution with the nonlinearity strength (for relatively large values of $|\chi|$), depending on the interpeak distance. As it is shown in the Appendix, if the separation of the two peaks in the 2D lattice is given by S_x and S_y , then

$$\lambda_u = \sqrt{1 + S_x S_y} \ 2^{(S_x + S_y)/2} |\chi|^{1 - \frac{S_x + S_y}{2}}, \quad \text{for } |\chi| \gg 1. \quad (32)$$

Fig. 9 presents numerical results in the case of $\chi < 0$ regarding the magnitude of instability of symmetric DP states with different interpeak separations S_x, S_y (points), as well as a comparison with the power-law (32).

Besides the pair of stable or unstable discrete eigenvalues, there is also the band of eigenvalues extending approximately from $\frac{|\chi|}{2} - 4$ to $\frac{|\chi|}{2} + 4$, except for the cases where the two peaks are located in first neighboring sites. Then,

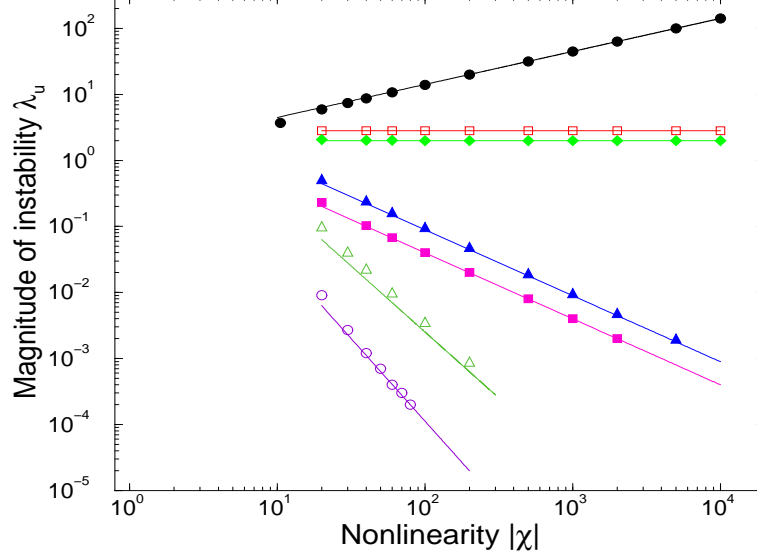


Fig. 9. Magnitude of instability λ_u of symmetric double-peaked solutions of DNLS for $\chi < 0$ in 2D (points) as a function of the strength of nonlinearity $|\chi|$, for various interpeak separations. Results for solutions along a lattice axis with $S_x = 1, S_y = 0$ (filled circles), $S_x = 2, S_y = 0$ (filled diamonds), $S_x = 4, S_y = 0$ (filled squares), $S_x = 7, S_y = 0$ (open circles), and along the diagonal with $S_x = S_y = 1$ (open squares), $S_x = S_y = 2$ (filled triangles), and $S_x = S_y = 3$ (open triangles), are presented. Lines show the power-law relation, Eq.(32), derived for large values of $|\chi|$.

for the symmetric states the band extends from $\frac{|\chi|}{2} - 3$ to $\frac{|\chi|}{2} + 5$, while for the antisymmetric states extends from $\frac{|\chi|}{2} - 5$ to $\frac{|\chi|}{2} + 3$. As $|\chi|$ decreases, the band moves towards zero and the states which are stable at large $|\chi|$ become unstable when the band collides with the discrete eigenvalues lying on the real axis.

5.3 Quadruple-peaked solutions

In this subsection QP solutions of high symmetry are presented, where their four peaks are on lattice sites forming a square of edge equal to l lattice constants. Such solutions may be symmetric, antisymmetric along both lattice axes, or symmetric along the one axis and antisymmetric along the other one, and at various interpeak distances l .

The former are calculated from the initial state

$$\psi_{n_x, n_y}^{(r=0)} = \frac{1}{\sqrt{4}} (\delta_{n_x, n_1} \delta_{n_y, n_2} + \delta_{n_x, n_1} \delta_{n_y, n_2+l} + \delta_{n_x, n_1+l} \delta_{n_y, n_2+l} + \delta_{n_x, n_1+l} \delta_{n_y, n_2}). \quad (33)$$

Fig. 10 shows such symmetric stationary states for $l = 1, 2$, and 3. The

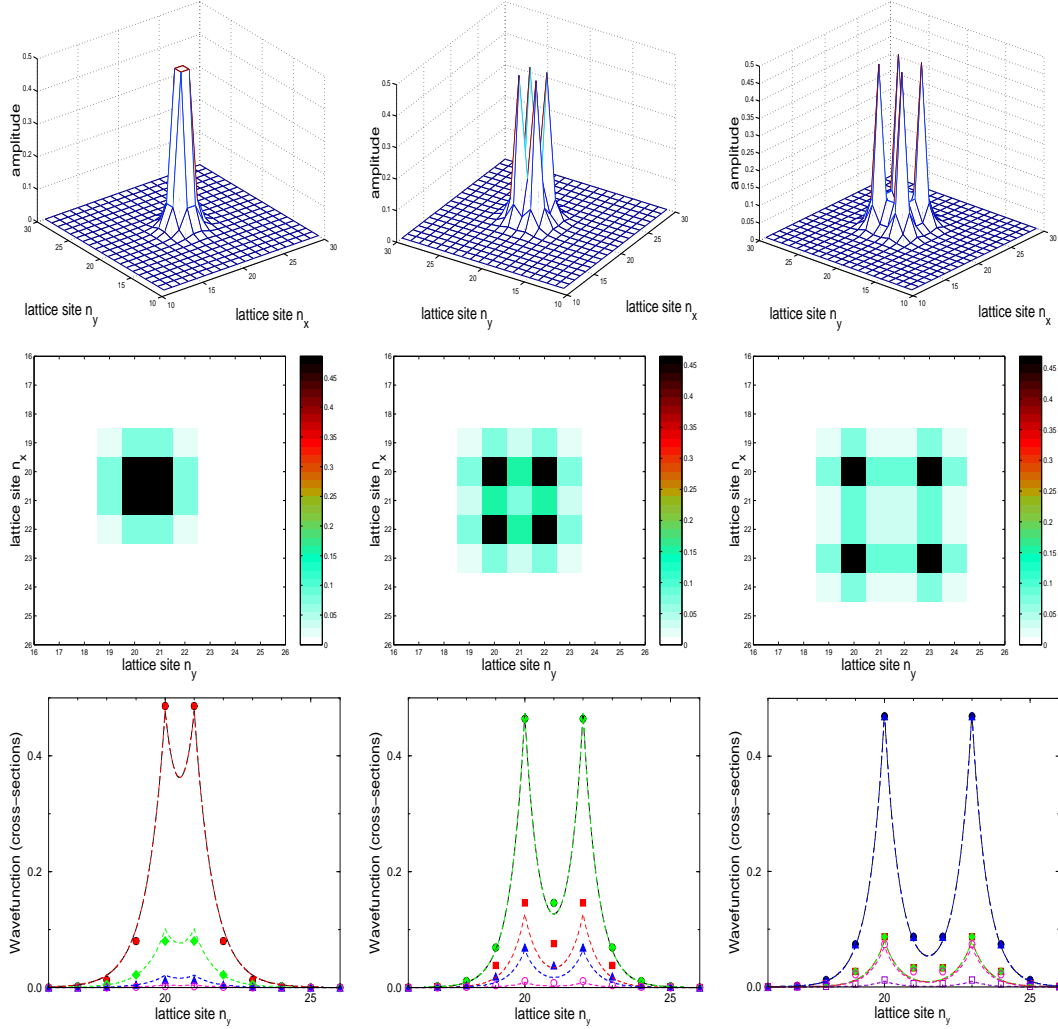


Fig. 10. 3D plots (first row) and density plots (second row) of quadruple-peaked symmetric solutions of DNLS in 2D. *Left column*: interpeak separation $l = 1$ lattice site, $\chi = -22.5$. *Middle column*: interpeak separation $l = 2$ sites, $\chi = -32$. *Right column*: interpeak separation $l = 3$ sites, $\chi = -30$. Cross-sections of the wavefunction are shown in the third row with points: $\psi_{n_x=n_1, n_y}$ (filled circles), $\psi_{n_x=n_1+1, n_y}$ (filled squares), $\psi_{n_x=n_1+2, n_y}$ (filled diamonds), $\psi_{n_x=n_1+3, n_y}$ (filled triangles), $\psi_{n_x=n_1+4, n_y}$ (open circles), $\psi_{n_x=n_1+5, n_y}$ (open squares, in the third column), where $n_1 = 20$ is the x -coordinate of the first peak. Dashed lines show analytical approximations of the solutions using Eq. (36).

solutions with $l = 1$ give the single branch with frequencies around $\omega = \frac{\chi}{4} - 2$ in Fig. 5. These solutions are unstable for negative χ . Linear stability analysis shows three purely imaginary pairs of opposite eigenvalues (two of these pairs are degenerate). For the case $l = 1$ ($l > 2$), as $|\chi|$ increases the magnitude of the unstable eigenvalues increases (decreases). For $l = 2$ the unstable eigenvalues approach constant values (around ± 2.83 the most unstable one and around ± 2 the doubly degenerate eigenvalues) for $|\chi| \gg 1$. However, for relatively large $\chi > 0$ the symmetric solutions corresponding to odd values of l are linearly

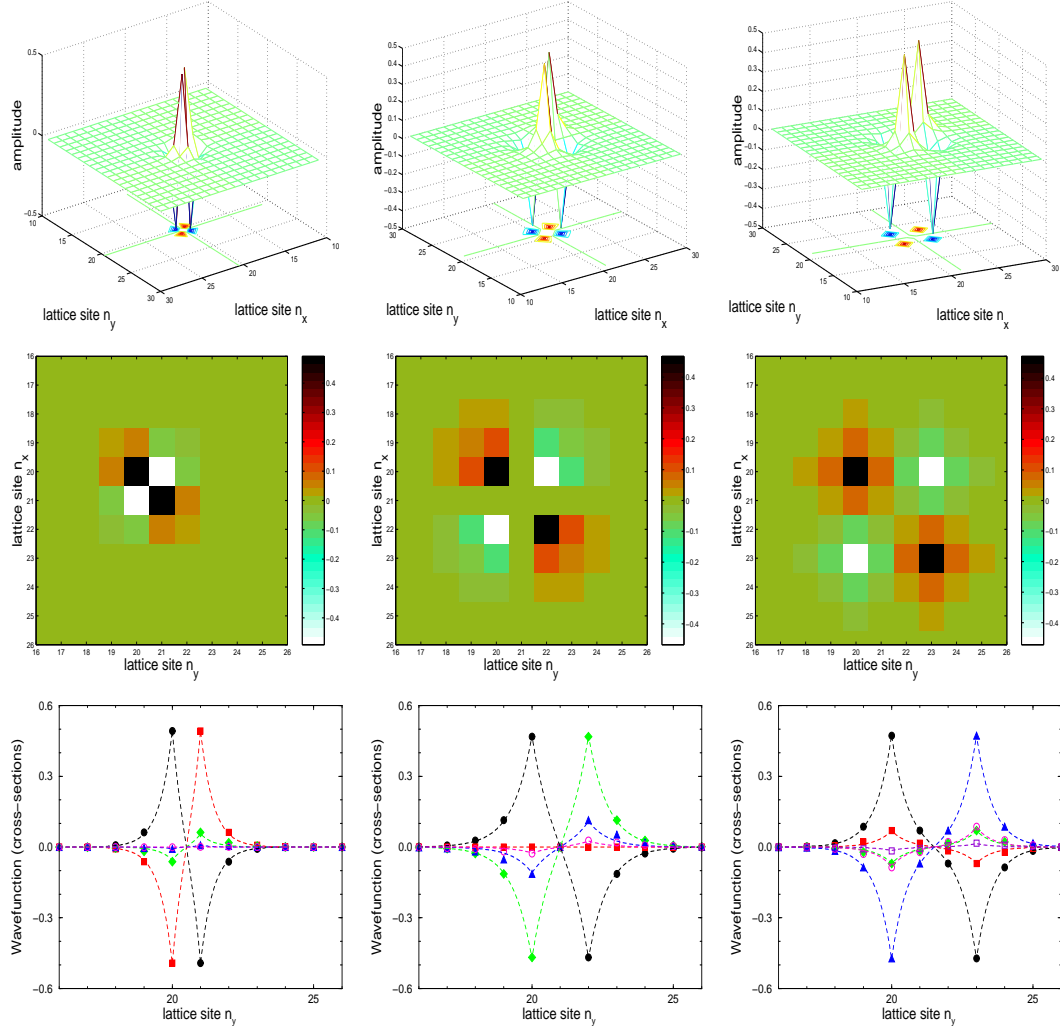


Fig. 11. 3D plots (first row) and density plots (second row) of quadruple-peaked antisymmetric solutions of DNLS in 2D. *Left column:* interpeak separation $l = 1$ lattice site, $\chi = -38$. *Middle column:* interpeak separation $l = 2$ sites, $\chi = -21$. *Right column:* interpeak separation $l = 3$ sites, $\chi = -26$. Cross-sections of the wavefunction are shown in the third row with points: $\psi_{n_x=n_1, n_y}$ (filled circles), $\psi_{n_x=n_1+1, n_y}$ (filled squares), $\psi_{n_x=n_1+2, n_y}$ (filled diamonds), $\psi_{n_x=n_1+3, n_y}$ (filled triangles), $\psi_{n_x=n_1+4, n_y}$ (open circles), $\psi_{n_x=n_1+5, n_y}$ (open squares, in the third column), where $n_1 = 20$ is the x -coordinate of the first peak. Dashed lines show analytical approximations of the solutions using Eq. (36).

stable with three real discrete pairs of eigenvalues. The band of eigenvalues extends approximately from $\frac{|\chi|}{4} - 4$ to $\frac{|\chi|}{4} + 4$, apart from the case of $l = 1$, where it extends from $\frac{|\chi|}{4} - 2$ to $\frac{|\chi|}{4} + 6$.

The antisymmetric along both axes QP solutions are obtained from alternating

signs on neighboring peaks:

$$\psi_{n_x, n_y}^{(r=0)} = \frac{1}{\sqrt{4}} (\delta_{n_x, n_1} \delta_{n_y, n_2} - \delta_{n_x, n_1} \delta_{n_y, n_2+l} + \delta_{n_x, n_1+l} \delta_{n_y, n_2+l} - \delta_{n_x, n_1+l} \delta_{n_y, n_2}). \quad (34)$$

Some examples are shown in Fig. 11. The branch of these solutions with $l = 1$ gives the single branch with frequencies around $\omega = \frac{\chi}{4} + 2$ in Fig. 5. For $\chi < 0$ these solutions are linearly stable for large values of $|\chi|$. In this case there exist three discrete real eigenvalues (two of them are degenerate) and the band extends from $\frac{|\chi|}{4} - 4$ to $\frac{|\chi|}{4} + 4$, apart from the case of $l = 1$, where it extends from $\frac{|\chi|}{4} - 6$ to $\frac{|\chi|}{4} + 2$. As long as the discrete eigenvalues are outside of the band the solution is linearly stable. When they collide instabilities develop. The dependence of the discrete eigenvalues on $|\chi|$ is the usual: for $l = 1$ ($l > 2$) they increase (decrease) with $|\chi|$, while for $l = 2$ they slightly vary, approaching constant values at $|\chi| \gg 1$. Regarding the solutions shown in Fig. 11 the last one (for $l = 3$, in the right column) is linearly stable and the other two are unstable. As previously, the opposite sign of χ ($\chi > 0$) does not change anything regarding the stability eigenvalues of symmetric and fully antisymmetric QP states, when l is even. On the contrary, for odd l these families of solutions interchange stability eigenvalues when $\chi \rightarrow -\chi$.

The last example of QP states, which are symmetric along one lattice axis and antisymmetric along the other one, are obtained from the initial state

$$\psi_{n_x, n_y}^{(r=0)} = \frac{1}{\sqrt{4}} (\delta_{n_x, n_1} \delta_{n_y, n_2} + \delta_{n_x, n_1} \delta_{n_y, n_2+l} - \delta_{n_x, n_1+l} \delta_{n_y, n_2+l} - \delta_{n_x, n_1+l} \delta_{n_y, n_2}). \quad (35)$$

Three cases (for $l = 1, 2$, and 3) are presented in Fig. 12. These solutions are always unstable since there are two pairs of purely imaginary eigenvalues $\pm i\beta$ and $\pm i\gamma$. There is also a discrete eigenvalue δ which is real for large values of $|\chi|$, but when it collides with the band (which extends approximately from $\frac{|\chi|}{4} - 4$ to $\frac{|\chi|}{4} + 4$) one more instability is developed. For $|\chi| \gg 1$, β and δ tend to the same value and they show the typical dependence on $|\chi|$: they increase (decrease) for $l = 1$ ($l > 2$) and they tend to 2 for $l = 2$. This picture does not change for positive χ , regardless whether l is even or odd.

In Fig. 5 branches of solutions of the symmetry obtained from (33) and (34) are shown for $l = 1, 2, 3, 4, 5, 6, 7, 10$, and 11 and from (35) for $l = 1, 2, 3, 4, 5, 10$, and 11 . Of course there are many more quadruplets having their four peaks in a rectangle or in random lattice sites, with any combination of signs, which are congested around the middle quasi-degenerate branch of the QP solutions of Fig. 5. An example of antisymmetric along *both diagonals* QP solution, forming a square with its edges (of length equal to $\sqrt{2}$) not along the axes, as the states presented above, but along the diagonals, is reported as a quasivortex in Ref. [36]

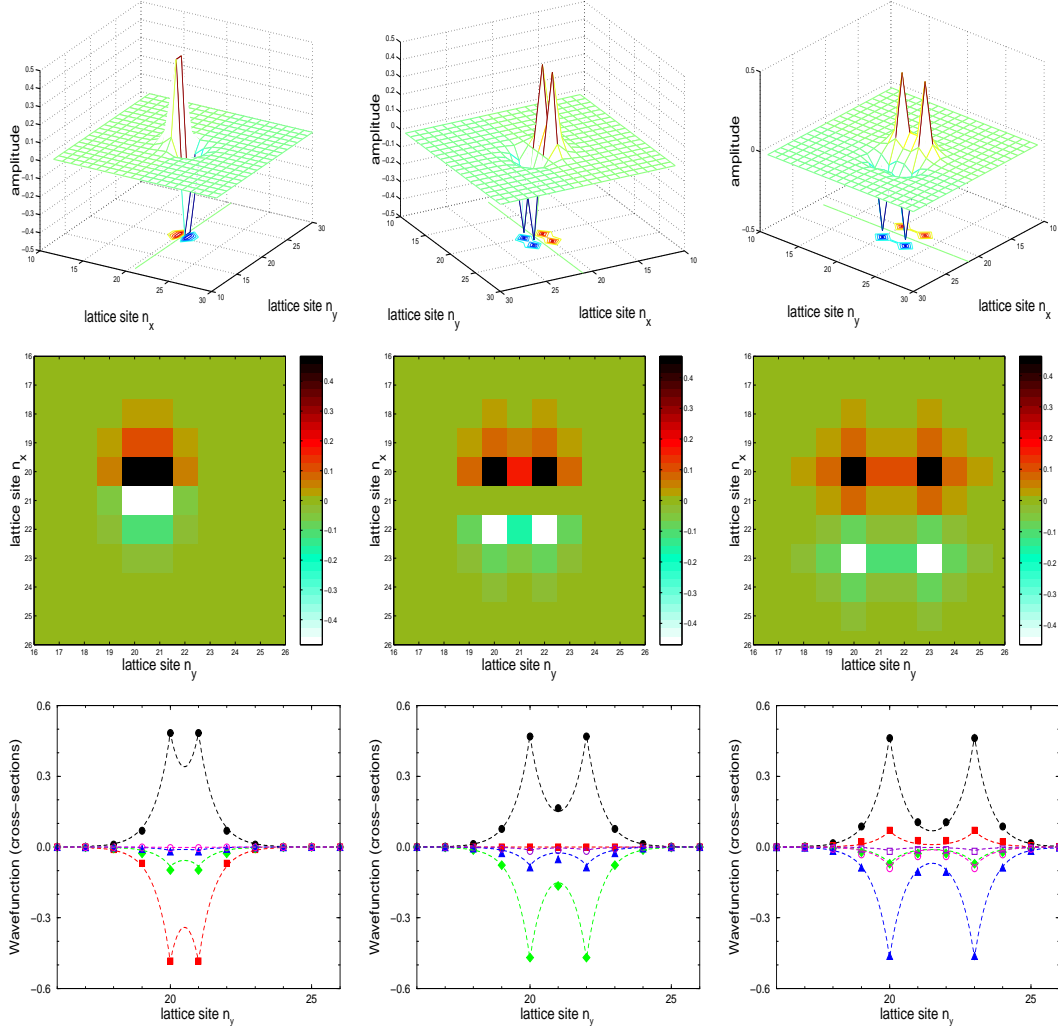


Fig. 12. 3D plots (first row) and density plots (second row) of quadruple-peaked symmetric/antisymmetric solutions of DNLS in 2D. *Left column:* interpeak separation $l = 1$ lattice site, $\chi = -27$. *Middle column:* interpeak separation $l = 2$ sites, $\chi = -27.5$. *Right column:* interpeak separation $l = 3$ sites, $\chi = -26$. Cross-sections of the wavefunction are shown in the third row with points: $\psi_{n_x=n_1, n_y}$ (filled circles), $\psi_{n_x=n_1+1, n_y}$ (filled squares), $\psi_{n_x=n_1+2, n_y}$ (filled diamonds), $\psi_{n_x=n_1+3, n_y}$ (filled triangles), $\psi_{n_x=n_1+4, n_y}$ (open circles), $\psi_{n_x=n_1+5, n_y}$ (open squares, in the third column), where $n_1 = 20$ is the x -coordinate of the first peak. Dashed lines show analytical approximations of the solutions using Eq. (37).

Once more, approximate analytical expressions can be derived for the QP solutions in 2D, by superimposing four single-peaked solutions of Eq. (12), each one corresponding to $\frac{\chi}{4}$. Regarding the high symmetry solutions presented above, if (n_1, n_2) is the position of the first peak and l the interpeak distance along the lattice axes ($l > 0$), then these stationary states can be approximated by

$$\psi_{n_x, n_y}^{QP} = \frac{1}{2\sqrt{1 \pm 2P + P^2}} \frac{1 - \zeta^2}{1 + \zeta^2} \left(\zeta^{|n_x - n_1| + |n_y - n_2|} \pm (-\text{sgn}\chi)^l \zeta^{|n_x - n_1| + |n_y - n_2 - l|} \right. \\ \left. + \zeta^{|n_x - n_1 - l| + |n_y - n_2 - l|} \pm (-\text{sgn}\chi)^l \zeta^{|n_x - n_1 - l| + |n_y - n_2|} \right) \quad (36)$$

and

$$\psi_{n_x, n_y}^{QP} = \frac{1}{2\sqrt{1 - P^2}} \frac{1 - \zeta^2}{1 + \zeta^2} \left(\zeta^{|n_x - n_1| + |n_y - n_2|} + \zeta^{|n_x - n_1| + |n_y - n_2 - l|} \right. \\ \left. - \zeta^{|n_x - n_1 - l| + |n_y - n_2 - l|} - \zeta^{|n_x - n_1 - l| + |n_y - n_2|} \right), \quad (37)$$

$$\text{where } P = (-\text{sgn}\chi)^l \frac{(1 + l)\zeta^l - (l - 1)\zeta^{l+2}}{1 + \zeta^2} \quad (38)$$

$$\text{and } \zeta = -\frac{1}{\chi/4} - \frac{6}{(\chi/4)^3} = -\frac{4}{\chi} - \frac{384}{\chi^3}. \quad (39)$$

Plus (minus) signs in Eq. (36) provide the symmetric (fully antisymmetric along both axes) QP solutions, except when χ is positive and l odd, where it is the reverse. Eq. (37) gives the solutions which are symmetric along one axis and antisymmetric along the other one, like those of Fig. 12. $P = \sum_{n_x, n_y} \psi_{n_x, n_y}^{SP[n_1, n_2]}(\frac{\chi}{4}) \psi_{n_x, n_y}^{SP[n_1, n_2 + l]}(\frac{\chi}{4})$ is the overlap of two neighboring single-peaked states at distance l . The overlap of two single-peaked states across the diagonal of the square, $\sum_{n_x, n_y} \psi_{n_x, n_y}^{SP[n_1, n_2]}(\frac{\chi}{4}) \psi_{n_x, n_y}^{SP[n_1 + l, n_2 + l]}(\frac{\chi}{4})$, is equal to P^2 . Cross-sections of Eqs. (36) and (37) are shown in the third rows of Figs. 10-12 with dashed lines.

6 Conclusions

Multi-peaked localized excited states are discussed for the one- and two-dimensional discrete nonlinear Schrödinger equation. Their numerical calculation is achieved by iterations of a simple map, where trivial initial states rapidly converge to the desired solution. Examples have been presented of symmetric and antisymmetric states with different interpeak separations for double-peaked solutions in 1D, as well as for double-peaked states along a lattice axis or along the diagonal and quadruple-peaked states on a square in 2D. Analytical approximations and the linear stability of the solutions have been discussed. For strong nonlinearities, the symmetric double-peaked states are unstable and the antisymmetric linearly stable, except for the case of positive nonlinearity and odd interpeak separation, where the situation is reversed. An interesting application that such multi-peaked solutions may have, concerns their potential use for information encoding and transfer in optical lattices

[37]. Multi-peaked solutions have been also discussed in different contexts [38,39,40].

The classification of these stationary states is based on their origin at the anti-continuous limit, even though sometimes their name may be misleading. For example, the symmetric double-peaked states in 1D and 2D and the symmetric quadruplet in 2D with interpeak separations equal to one lattice constant, can be viewed as solutions having one peak. However, this classification is very useful for organizing the discrete frequency and energy spectrum of DNLS. The concept of anti-continuous limit [23] facilitates the interpretation of the structure of this spectrum.

Some of the stationary states presented in this work have been also discussed in other studies and different names are attributed to them. The double-peaked solution in 1D with interpeak separation $S = 1$ has been named Page mode, even mode, or centered-between-sites [41]. Antisymmetric double-peaked states in 1D with $S = 1$ or $S = 2$ are also known as twisted modes [42], while their analogues in 2D with their peaks along the diagonal have been discussed in [43]. In Ref. [44] the symmetric double-peaked state along a lattice axis with $S = 1$ in 2D and the symmetric quadruple-peaked state with interpeak separation $l = 1$ have been named hybrid mode and Page-like mode, respectively. The double-peaked symmetric stationary solution along the diagonal with $l = 1$ in 2D has been also known [45].

Acknowledgements

The author would like to thank S. Aubry for useful and stimulating suggestions, R. Vicencio and M. Johansson for interesting discussions and for bringing to his attention relevant references, and the referees for useful comments. This work is dedicated to Serge on the occasion of his 60th birthday, with a strong appreciation for the valuable knowledge and fruitful ideas that he has tried to communicate to us and many wishes for even more breakthroughs on nonlinear physics in the future.

Appendix A

A.1 Linear stability of a stationary state

Considering small deviations $\delta\psi_n(t)$ from a stationary solution of Eq. (5), i.e. $\Psi_n(t) = (\psi_n + \delta\psi_n(t)) \cdot e^{-i\omega_0 t}$ (where ψ_n is time-independent and real and ω_0 is the corresponding frequency), substituting in DNLS Eq. (1), and linearizing

in respect to the complex small perturbations $\delta\psi_n(t)$, one obtains

$$i\frac{d\delta\psi_n}{dt} = (-\omega_0 + \chi\psi_n^2)\delta\psi_n - \sum_{\delta} \delta\psi_{n+\delta} + 2\chi\psi_n^2 \text{Re}(\delta\psi_n), \quad (40)$$

where $\text{Re}(\delta\psi_n)$ is the real part of $\delta\psi_n(t)$. Substituting solutions of the form

$$\delta\psi_n(t) = a_n \sin(\omega t) + ib_n \cos(\omega t) \quad (41)$$

in the linearized equation (40), yields the following coupled system

$$\omega a_n = (-\omega_0 + \chi\psi_n^2)b_n - \sum_{\delta} b_{n+\delta} \quad (42)$$

$$\omega b_n = (-\omega_0 + 3\chi\psi_n^2)a_n - \sum_{\delta} a_{n+\delta}. \quad (43)$$

This implies that the stability eigenvalues ω can be obtained as the eigenvalues of the $2L \times 2L$ (where L is the total number of lattice sites) matrix M :

$$M \begin{pmatrix} A \\ B \end{pmatrix} = \begin{pmatrix} \theta & M_1 \\ M_2 & \theta \end{pmatrix} \begin{pmatrix} A \\ B \end{pmatrix} = \omega \begin{pmatrix} A \\ B \end{pmatrix}, \quad (44)$$

where the $2L \times 1$ column $(A, B)^T \equiv (a_1, \dots, a_L, b_1, \dots, b_L)^T$ corresponds to the eigenvectors, θ denotes the $L \times L$ zero matrix and M_1, M_2 are the tight-binding $L \times L$ matrices given through the right-hand-sides of Eqs. (42) and (43), respectively. M_1 and M_2 differ only in their diagonal elements; $M_{1,ii} = -\omega_0 + \chi\psi_i^2$ and $M_{2,ii} = -\omega_0 + 3\chi\psi_i^2$, while the non-diagonal matrix elements are zero, except when they correspond to first neighboring sites where they are equal to -1 .

From Eq. (41) we see that if there is an eigenvalue of M with non-zero imaginary part, then the stationary solution is unstable. It can be easily verified that any stationary solution has a stability eigenvalue $\omega = 0$, with eigenvector $a_n = 0, b_n = \psi_n$, since Eq. (43) is trivially satisfied and Eq. (6) provides a solution making zero the right-hand-side of (42). The eigenvalue $\omega = 0$ is doubly degenerate possessing a second eigenvector known as growth mode [8].

A.2 Obtaining the linear stability eigenvalues through a tight-binding Hamiltonian

Here it is shown that the eigenvalues of the linear stability problem can be calculated through the energy eigenvalues and eigenvectors of a tight-binding

Hamiltonian² with an on-site potential determined by the stationary state ψ_n . In particular, consider the Hamiltonian eigenvalue problem

$$H_l \phi_n^\nu = - \sum_{\delta} \phi_{n+\delta}^\nu + U_n \phi_n^\nu = E_\nu \phi_n^\nu, \quad \text{with potential } U_n = \chi \psi_n^2, \quad (45)$$

where E_ν and ϕ_n^ν are the eigenvalues and the corresponding eigenvectors. The potential U_n has the shape of the stationary state under discussion, multiplied by the nonlinearity parameter. Comparing Eqs. (6) and (45) one obtains that ψ_n is an eigenvector $\phi_n^{\nu=0}$ of H_l with $E_{\nu=0} = \omega_0$.

Expressing the eigenvectors a_n and b_n of the linear stability system (42), (43) in the complete basis ϕ_n^ν of the Hamiltonian H_l , i.e. $a_n = \sum_{\nu} a_\nu \phi_n^\nu$ and $b_n = \sum_{\nu} b_\nu \phi_n^\nu$, substituting in the system (42), (43), and using Eq. (45) and the relation $\sum_n \phi_n^\nu \phi_n^{\nu'} = \delta_{\nu,\nu'}$, yields that for $\nu \neq 0$ is $b_\nu = \frac{\omega}{E_\nu - E_0} a_\nu$ and

$$\left[(E_\nu - E_0) - \frac{\omega^2}{E_\nu - E_0} + 2\chi \sum_n (\phi_n^0 \phi_n^\nu)^2 \right] a_\nu + 2\chi \sum_{\nu' \neq \nu} a_{\nu'} \left(\sum_n (\phi_n^0)^2 \phi_n^\nu \phi_n^{\nu'} \right) = 0. \quad (46)$$

These $L-1$ equations (since $\nu \neq 0$) provide the $2L-2$ non-zero stability eigenvalues $\omega = \pm \sqrt{\omega^2}$. We see that the eigenvalues of the linear stability analysis appear as pairs of opposite sign and the ω^2 result from the diagonalization of the $(L-1) \times (L-1)$ matrix

$$K_{\nu,\nu'} = \left[(E_\nu - E_0)^2 + 2\chi(E_\nu - E_0) \sum_n (\phi_n^0 \phi_n^\nu)^2 \right] \delta_{\nu,\nu'} + (1 - \delta_{\nu,\nu'}) 2\chi(E_\nu - E_0) \sum_n (\phi_n^0)^2 \phi_n^\nu \phi_n^{\nu'}, \quad \text{where } \nu, \nu' \neq 0. \quad (47)$$

$K_{\nu,\nu'}$ is constructed from the eigenspectrum of H_l . Using this matrix, analytical results are obtained in the following subsection for the linear stability eigenvalues of double-peaked solutions of DNLS for large values of $|\chi|$, and the Eqs. (23) and (32) are derived.

A.3 Application: double-peaked stationary states close to the anti-continuous limit

For a DP stationary solution the potential U_n of Eq. (45) is a double well for negative χ and a double barrier for positive χ . If $|\chi| \gg 1$, then ψ_n is

² a similar procedure has been used in Ref. [16] for the linear stability of a slightly more complicated system, viz. the polarons of the adiabatic Holstein model

localized at almost two lattice sites, where the two peaks are located, and each well (barrier) of U_n is very deep (high) and narrow, with a strength about $\frac{\chi}{2}$. In this case the Hamiltonian H_l , Eq. (45), is equivalent to a tight-binding problem with two equal impurities with large on-site energies $\frac{\chi}{2}$. Then the energy spectrum has two discrete eigenvalues (the $E_0 = \omega_0$ and a second one, denoted by E_1) and, for an extended system, all the other eigenvalues belong to the continuous band from $-2d$ to $2d$ [46]. The eigenvectors of the continuous spectrum are proportional to $\frac{1}{\sqrt{L}}$ and therefore negligibly small at any lattice site. Since the sums over the lattice sites n that appear in $K_{\nu,\nu'}$ in Eq. (47) contain the tightly localized around two sites wavefunction $\phi_n^0 \equiv \psi_n$, they can be neglected when they involve an eigenstate of the continuous. The $\phi_n^\nu, \phi_n^{\nu'}$ of $K_{\nu,\nu'}$ do not include the $\nu = 0$ and thus there is only one localized eigenstate among them; the ϕ_n^1 corresponding to E_1 . As a result the non-diagonal matrix elements of $K_{\nu,\nu'}$ can be neglected, since they contain products of two eigenstates $\phi_n^\nu \phi_n^{\nu'}$ and at least one of them it belongs to the continuum. The diagonal ones, providing directly the stability eigenvalues ω^2 , are

$$\omega^2 = K_{\nu,\nu} = (E_\nu - E_0)^2, \quad \text{for } \nu \neq 1 \quad \text{and} \quad (48)$$

$$\omega^2 = K_{1,1} = (E_1 - E_0)^2 + 2\chi(E_1 - E_0) \sum_n (\phi_n^0 \phi_n^1)^2, \quad \text{for } \nu = 1 \quad (49)$$

Eq. (48) gives two bands of real eigenvalues $\omega = \pm|E_\nu - E_0|$, symmetrically positioned around zero, and Eq. (49) a discrete pair of eigenvalues $\omega = \pm\sqrt{K_{1,1}}$.

The discrete eigenspectrum of H_l is given by

$$\phi_n^\pm = \frac{1}{\sqrt{2(1 \pm P)}} \left(g_n^{[n_0]} \pm (-sgn\chi)^S g_n^{[n_0+S]} \right) \longrightarrow E_\pm = \frac{\epsilon \pm v}{1 \pm P} \approx \epsilon \pm v \mp \epsilon P, \quad (50)$$

where $g_n^{[n_0]}, g_n^{[n_0+S]}$ represent single-peaked wavefunctions, centered at n_0 and $n_0 + S$, respectively. Here, n , n_0 , and S (S or its components are assumed positive) have to be understood as integers in 1D and pairs or sums of integers in 2D, e.g. $n \rightarrow (n_x, n_y)$, $n_0 \rightarrow (n_1, n_2)$, $S \rightarrow (S_x, S_y)$, $(-sgn\chi)^S \rightarrow (-sgn\chi)^{S_x+S_y}$, etc. The other quantities in the energy eigenvalues E_\pm of Eq. (50) are $\epsilon = \langle g_n^{[n_0]} | H_l | g_n^{[n_0]} \rangle = \langle g_n^{[n_0+S]} | H_l | g_n^{[n_0+S]} \rangle$ and the small overlap integrals $v = (-sgn\chi)^S \langle g_n^{[n_0]} | H_l | g_n^{[n_0+S]} \rangle$ and $P = (-sgn\chi)^S \langle g_n^{[n_0]} | g_n^{[n_0+S]} \rangle$. For χ negative, i.e. attractive potential U_n , the upper (lower) signs in Eq. (50) correspond to the ground (first excited) state of H_l , while for positive χ , i.e. repulsive U_n , they provide the highest-energy (second highest-energy) state. Note that for positive χ and odd S the highest-energy state is the antisymmetric one because of the $(-sgn\chi)^S$ term in (50), in contrary to the case of even S . It is convenient to distinguish three cases:

- (i) negative χ ,
- (ii) positive χ and even S (or even $S_x + S_y$), and
- (iii) positive χ and odd S (or odd $S_x + S_y$).

For symmetric DP stationary states ψ_n , the ϕ_n^+, E_+ of Eq. (50) correspond to $\phi_n^0 \equiv \psi_n$ and E_0 and the ϕ_n^-, E_- to ϕ_n^1 and E_1 in cases (i) and (ii), while it is the other way around in case (iii). For antisymmetric DP states ψ_n , holds the opposite: the ϕ_n^-, E_- correspond to ϕ_n^0 and E_0 and the ϕ_n^+, E_+ to ϕ_n^1 and E_1 in cases (i) and (ii), and the reverse is valid in case (iii).

The discrete eigenvalue (49) is dominated by the second term, since $E_1 - E_0$ is a small quantity and $\chi \gg 1$. For a symmetric DP solution $E_1 - E_0$ is positive in cases (i) and (iii) and negative in case (ii). Therefore, $K_{1,1}$, which has the same sign as $\chi(E_1 - E_0)$, is negative (positive) in cases (i) and (ii) (in case (iii)), meaning that the symmetric DP solution is unstable (linearly stable) with a pair of purely imaginary (real) discrete eigenvalues. The situation is reverse for an antisymmetric DP stationary state since $E_1 - E_0$ has the opposite sign now. Thus, when the symmetric DP solution is linearly stable (unstable) the antisymmetric one is unstable (linearly stable). These results are confirmed by the numerical simulations of sections 4 and 5. The above arguments about the linear stability/instability of a symmetric or antisymmetric DP solution of DNLS close to the anti-continuous limit, are generally applied at any dimension. Therefore, one expects that, for large $|\chi|$, also in 3D an antisymmetric DP stationary state is linearly stable and a symmetric unstable, except when χ is positive and the interpeak distance $S_x + S_y + S_z$ is odd, where they interchange roles regarding their stability.

The previous discussion can be quantified and using Eqs. (49) and (50) analytical expressions are obtained for the discrete pair of eigenvalues in the limit of $|\chi| \gg 1$. The wavefunctions g_n in (50) are given by Eq. (12) for $\frac{\chi}{2}$. Taking into account that $\zeta = -\frac{2}{\chi}$ one obtains to leading order: $P = (-sgn\chi)^S(1+S)\zeta^S$ in 1D and $P = (-sgn\chi)^{S_x+S_y}(1+S_x)(1+S_y)\zeta^{S_x+S_y}$ in 2D [see also Eqs. (19) and (30)], the sum $\sum_n (\phi_n^0 \phi_n^1)^2 = \frac{1}{2}$, the coupling $v = (-sgn\chi)^S(-S\zeta^{S-1} + \chi\zeta^S)$ in 1D and $v = (-sgn\chi)^{S_x+S_y}[-(S_x + S_y + 2S_x S_y)\zeta^{S_x+S_y-1} + \chi\zeta^{S_x+S_y}]$ in 2D, and the on-site energy $\epsilon = \frac{\chi}{2}$. Then for symmetric DP states in 1D is $E_1 - E_0 = -2(v - \epsilon P) = \frac{2^S}{|\chi|^{S-1}}$ in case (i), $E_1 - E_0 = -2(v - \epsilon P) = -\frac{2^S}{\chi^{S-1}}$ in case (ii), and $E_1 - E_0 = 2(v - \epsilon P) = \frac{2^S}{\chi^{S-1}}$ in case (iii). The signs are the same in 2D, but the magnitudes change to $\frac{(1+S_x S_y)2^{S_x+S_y}}{|\chi|^{S_x+S_y-1}}$. Therefore Eq. (49) yields that in cases (i) and (ii) $\omega^2 = -\frac{2^S}{|\chi|^{S-2}}$ in 1D and $\omega^2 = -\frac{(1+S_x S_y)2^{S_x+S_y}}{|\chi|^{S_x+S_y-2}}$ in 2D, while in case (iii) ω^2 is positive with the same magnitude. For the antisymmetric DP states the $E_1 - E_0$ and consequently the ω^2 are the same like previously, but with opposite sign. As a result the discrete eigenvalues are

$$\omega = \pm i 2^{S/2} |\chi|^{1-S/2} \text{ in 1D and } \omega = \pm i \sqrt{1 + S_x S_y} 2^{(S_x+S_y)/2} |\chi|^{1-\frac{S_x+S_y}{2}} \text{ in 2D} \quad (51)$$

for the (unstable) symmetric DP states in cases (i) and (ii) and the antisymmetric in case (iii), while

$$\omega = \pm 2^{S/2} |\chi|^{1-S/2} \text{ in 1D and } \omega = \pm \sqrt{1 + S_x S_y} 2^{(S_x + S_y)/2} |\chi|^{1 - \frac{S_x + S_y}{2}} \text{ in 2D} \quad (52)$$

for the (linearly stable) symmetric states in case (iii) and the antisymmetric ones in cases (i) and (ii). Eq. (51) provides the instability magnitudes given in Eqs. (23) and (32), while Eq. (52) the stable eigenvalue used in Eq. (24). By decreasing $|\chi|$, as the stationary state ψ_n and the potential U_n of (45) become more extended, additional discrete levels of H_l may appear, resulting in additional discrete eigenvalues of the linear stability problem.

For the DP states, $E_0 \equiv \omega_0$ equals, to leading order, to $\epsilon = \frac{\chi}{2}$. The next corrections are $\pm(v - \epsilon P)$, which are equal to $\pm \frac{E_1 - E_0}{2} = \pm \frac{2^{S-1}}{|\chi|^{S-1}}$ in 1D and a similar expression in 2D (see above). These corrections are inverse powers of χ , apart from the case of $S = 1$ (or $S_x + S_y = 1$). Then, if $\chi < 0$ for example, the symmetric DP states have $E_0 \equiv \omega_0 = \frac{\chi}{2} + (v - \epsilon P) = \frac{\chi}{2} - 1$ and the antisymmetric have $E_0 \equiv \omega_0 = \frac{\chi}{2} - (v - \epsilon P) = \frac{\chi}{2} + 1$ (see the lower and upper branches of DP states in Figs. 1 and 5, while similar is the case for the single branches of the QP states presented in 2D). The knowledge of E_0 and the continuous band of H_l (from $-2d$ to $2d$) provides the bands of stability eigenvalues $\omega = \pm |E_\nu - E_0|$, Eq. (48). The latter, for positive ω , extends from $\frac{|\chi|}{2} - 2d$ to $\frac{|\chi|}{2} + 2d$, apart from the case of $S = 1$ (or $S_x + S_y = 1$), where it extends between $\frac{|\chi|}{2} \pm 1 - 2d$ and $\frac{|\chi|}{2} \pm 1 + 2d$ (the upper signs correspond to symmetric DP states in cases i) and ii) and antisymmetric in case iii), while the minus signs correspond to the complementary situations). These results are in accordance with the numerical observations in sections 4 and 5.

References

- [1] J.C. Eilbeck, P.S. Lomdahl, and A.C. Scott, *Physica D* **16**, 318 (1985).
- [2] J.C. Eilbeck in *Davydov's Soliton Revisited*, edited by P.L. Christiansen and A.C. Scott (Plenum Press, NY, 1990), p. 473.
- [3] R.S. MacKay and S. Aubry, *Nonlinearity* **7**, 1623 (1994).
- [4] M. Johansson and S. Aubry, *Nonlinearity* **10**, 1151 (1997).
- [5] S. Flach, K. Kladko, and R.S. MacKay, *Phys. Rev. Lett.* **78**, 1207 (1997).
- [6] D. Hennig and G.P. Tsironis, *Phys. Rep.* **307**, 334 (1999).
- [7] K.Ø. Rasmussen, S. Aubry, A.R. Bishop, and G.P. Tsironis, *Eur. Phys. J. B* **15**, 169 (2000).
- [8] M. Johansson and S. Aubry, *Phys. Rev. E* **61**, 5864 (2000).

- [9] J.M. Bergamin, T. Bountis, and C. Jung, J. Phys. A: Math. Gen. **33**, 8059 (2000).
- [10] A.R. Bishop, G. Kalosakas, K.Ø. Rasmussen, and P.G. Kevrekidis, Chaos **13**, 588 (2003).
- [11] R.A. Vicencio, M.I. Molina, and Y.S. Kivshar, Opt. Lett. **28**, 1942 (2003).
- [12] J. Cómez-Gardeñes, F. Falo, and L.M. Floría, Phys. Lett. A **332**, 213 (2004).
- [13] A.C. Scott and J.C. Eilbeck, Chem. Phys. Lett. **132**, 23 (1986).
- [14] D.N. Christodoulides and R.I. Joseph, Opt. Lett. **13**, 794 (1988).
- [15] T. Holstein, Ann. Phys. (N.Y.) **8**, 325 (1959).
- [16] G. Kalosakas, S. Aubry, and G.P. Tsironis, Phys. Rev. B **58**, 3094 (1998).
- [17] A.S. Davydov and N.I. Kislukha, Phys. Stat. Sol. (b) **59**, 465 (1973).
- [18] A. Scott, Phys. Rep. **217**, 1 (1992).
- [19] A.V. Zolotaryuk, K.H. Spatschek, and O. Kluth, Phys. Rev. B **47**, 7827 (1993).
- [20] A. Trombettoni and A. Smerzi, Phys. Rev. Lett. **86**, 2353 (2001).
- [21] G. Kalosakas, K.Ø. Rasmussen, and A.R. Bishop Phys. Rev. Lett. **89**, 030402 (2002).
- [22] A.M. Morgante, M. Johansson, G. Kopidakis, and S. Aubry, Physica D **162**, 53 (2002).
- [23] S. Aubry, Physica D **71**, 196 (1994).
- [24] N.K. Voulgarakis and G.P. Tsironis, Phys. Rev. B **63**, 014302 (2000).
- [25] N.K. Voulgarakis, G. Kalosakas, A.R. Bishop, and G.P. Tsironis, Phys. Rev. B **64**, 020301 (2001).
- [26] D. Hennig, Phys. Rev. E **64**, 041908 (2001); Eur. Phys. J. B **24**, 377 (2001); Phys. Rev. B **65**, 174302 (2002).
- [27] S. Komarnicki and D. Hennig, J. Phys.: Cond. Matt. **15**, 441 (2003).
- [28] D. Hennig, E.B. Starikov, J.F.R. Archilla, and F. Palmero, J. Biol. Phys. **30**, 227 (2004).
- [29] S. Aubry and P. Quemerais, in *Low-Dimensional Electronic Properties of Molybdenum Bronzes and Oxides*, edited by C. Schlenker (Kluwer Academic, Dordrecht, 1989), p. 295.
- [30] S. Aubry, G. Abramovici, and J.-L. Raimbault, J. Stat. Phys. **67**, 675 (1992).
- [31] S. Aubry, in *Phase Separation in Cuprate Superconductors*, edited by K.A. Müller and G. Benedek (World Scientific, Singapore, 1993), p. 304.

- [32] G.L. Alfimov, V.A. Brazhnyi, and V.V. Konotop, *Physica D* **194**, 127 (2004).
- [33] E.W. Laedke, O. Kluth, and K.H. Spatschek, *Phys. Rev. E* **54**, 4299 (1996).
- [34] T. Kapitula, P.G. Kevrekidis, and B.A. Malomed, *Phys. Rev. E* **63**, 036604 (2001).
- [35] D.E. Pelinovsky, P.G. Kevrekidis, and D.J. Frantzeskakis, arXiv:nlin.PS/0410005.
- [36] P.G. Kevrekidis, B.A. Malomed, Z. Chen, and D.J. Frantzeskakis, *Phys. Rev. E* **70**, 056612 (2004).
- [37] Y.V. Kartashov, A.A. Egorov, L. Torner, and D.N. Christodoulides, *Opt. Lett.* **29**, 1918 (2004).
- [38] L.S. Brizhik and A.A. Eremko, *Physica D* **81**, 295 (1995).
- [39] M.A. Fuentes, P. Maniadis, G. Kalosakas, K.Ø. Rasmussen, A.R. Bishop, V.M. Kenkre, and Y.B. Gaididei, *Phys. Rev. E* **70**, 025601 (2004).
- [40] P. Panayotaros, "Multibreather solitons in the diffraction managed NLS equation", to appear in *Phys. Lett. A*.
- [41] Y.S. Kivshar and D.K. Campbell, *Phys. Rev. E* **48**, 3077 (1993).
- [42] S. Darmanyan, A. Kobayakov, and F. Lederer, *JETP* **86**, 682 (1998).
- [43] P.G. Kevrekidis, B.A. Malomed, and A.R. Bishop, *J. Phys. A: Math. Gen.* **34**, 9615 (2001).
- [44] P.G. Kevrekidis, K.Ø. Rasmussen, and A.R. Bishop, *Phys. Rev. E* **61**, 2006 (2000).
- [45] R. Vicencio, unpublished.
- [46] E.N. Economou, *Green's functions in quantum physics*, (Springer-Verlag, Berlin, 1990).